Stable Nickel(I) Complexes with Electron-Rich, Sterically-Hindered, Innocent PNP Pincer Ligands

Sébastien Lapointe[†], Eugene Khaskin[†], Robert R. Fayzullin[‡] and Julia R. Khusnutdinova*[†]

[†] Okinawa Institute of Science and Technology Graduate University, Coordination Chemistry and Catalysis Unit, 1919-1 Tancha, Onna-son, Okinawa, Japan, 904-0495

[‡] Arbuzov Institute of Organic and Physical Chemistry, FCR Kazan Scientific Center, Russian Academy of Sciences, 8 Arbuzov Street, Kazan 420088, Russian Federation

ABSTRACT: The electronic and steric properties of a new class of electron-rich and sterically hindered tertamethylated PNP pincer ligands (Me_4PNP^R = 2,6-bis[(dialkylphosphino)propyl]pyridine with R = ^{i}Pr, ^{t}Bu) are discussed. Introducing the methyl groups on the pincer arm prevents de-aromatization of the pincer framework and increases the bulkiness and electron-donating capacity of the ligand. Highly reactive Ni^I species are thus prevented from dimerizing and can be analyzed by a wide variety of spectroscopic methods. X-ray diffraction study shows that steric bulk has an important influence on the resulting geometric and spectroscopic properties of the Ni^I complexes. Complexes **5** and **6**, which contain ^{i}Pr groups on the phosphorus atoms, show a very rare see-saw geometry around the metal center, while ^{t}Bu complexes **7** and **8** show a distorted square-planar geometry. Computational analysis reveals the SOMO for all complexes has a $d_{x^2-y^2}$ character with the spin density mostly residing on the nickel.

INTRODUCTION

After the discovery and pioneering work by the groups of Shaw[1] and Van Koten[2, 3] in the 1970's, pincer ligands and their associated complexes have become a mature organometallic research field. Many different types of pincer ligands have been designed that vary in the donor atoms, steric or electronic influence substituents on the donors, and the rigidity of the ligand in general (PCP,[4-15] $POC_{sp2}OP$,[16-22] $POC_{sp3}OP$,[23] POCN,[24-28] PNP,[29-37] PONOP,[38-45] PIMCOP,[46] and NNN[47-49] amongst others). The highly versatile and often electron-donating nature of the pincer ligand framework allows for almost endless customization. Most pincer complex research has historically focused on second or third-row transition metals for their catalytic activities, or on stable oxidation states of first-row transition metals. In comparison, the interest in isolation of complexes with first-row transition metals in unusual oxidation states[24, 50-60] or the stabilization of highly reactive species[61-65] have only gained popularity recently. Over the last decade, pincer based paramagnetic organometallic complexes have played an increasing role in catalysis, with first-row transition metals adopting an increasingly important role.[66-68] In particular, the Ni^I oxidation state is paramagnetic and is less common than Ni^{II} and Ni^0, but has growing importance in catalysis,[69-78] coupling reactions,[70, 79-82] and is proposed to play an important role in enzymatic processes.[83-88]

While pincer complexes have been well studied over the past decades for Ni,[1, 17, 18, 42, 89-95] the ability of most classic pincer ligands to undergo Metal-Ligand Cooperation (MLC) can obscure metal-based reactivity and favor two-electron pathways.[96] In this regard, we have designed new, electron-rich ligands where any possible MLC is blocked by the addition of methyl groups on the pincer arm. The additional methyl groups also induces a highly sterically hindered environment, which limits substrate access to the metal center and prevents dimerization of complexes and intermolecular decomposition pathways. Thus, the ligand design principles also foresee that first-row, low-valent, mono-metallic complexes relevant to catalysis that are supported by these bulky ligands can be examined for pure, metal-based reactivity and their electronic properties can be studied more easily.

The importance of low-valent nickel to catalysis and the well-studied pincer examples of nickel complexes, led us to examine whether we can isolate Ni^I species. Gratifyingly, we found that our ligand framework readily affords Ni^I complexes, which are stable indefinitely at room temperature and whose structures vary based on the ligand's sterics. Accordingly, we find that the bulkier ^{t}Bu containing species **7** and **8** are closer to a square planar geometry while the ^{i}Pr containing species **5** and **6** adopt a very rare see-saw geometry. The new complexes were examined and characterized by electrochemistry, X-ray diffraction, UV-vis, EPR and DFT methods, showing that the geometry difference leads to drastically different spectroscopic features.

RESULTS AND DISCUSSION

Synthesis of ligands and Ni^{II} halide complexes. The bulky PNP ligands were synthesized by modification of the synthetic procedure for the previously reported unsubstituted PNP^RBH_3 ligands (R = ^{i}Pr, ^{t}Bu),[97] which also differs from a procedure for similar previously reported methylated ligands.[98] They were then reacted subsequently with *n*-butyl lithium and methyl iodide multiple times (Scheme 1) to afford the fully methylated **$Me_4PNP^RBH_3$** ligands in 83-85% yields.

Scheme 1. Preparation of Me_4PNP^R-BH_3 and Me_4PNP^R ligands

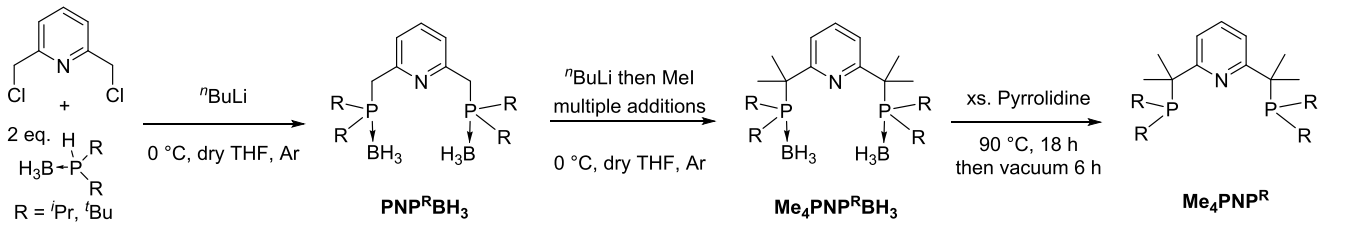

Scheme 2. Preparation of Nickel(II) cationic complexes [1] to [4]

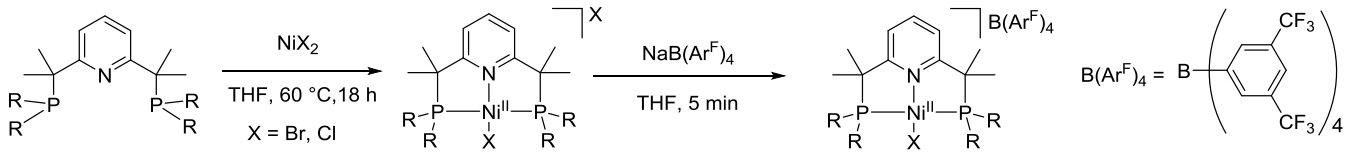

	Yield
R = ^{i}Pr, X = Br (**[1]Br**)	62 %
R = ^{i}Pr, X = Cl (**[2]Cl**)	69 %
R = ^{t}Bu, X = Br (**[3]Br**)	57 %
R = ^{t}Bu, X = Cl (**[4]Cl**)	85 %

	Yield
R = ^{i}Pr, X = Br (**[1]B(Ar^F)$_4$**)	100 %
R = ^{i}Pr, X = Cl (**[2]B(Ar^F)$_4$**)	88 %
R = ^{t}Bu, X = Br (**[3]B(Ar^F)$_4$**)	80 %
R = ^{t}Bu, X = Cl (**[4]B(Ar^F)$_4$**)	67 %

The tetramethylated **$Me_4PNP^RBH_3$** ligand is deprotected by reaction with pyrrolidine at 90 °C for 18 hours, and high vacuum application for 4-6 hours following the reaction allows for a thorough removal of the pyrrolidine-BH_3 complex formed. The resulting deprotected ligands (**Me_4PNP^R** ligand) were isolated in pure form and characterized by NMR spectroscopy, and XRD for **Me_4PNP^{tBu}**. The deprotected ligand **Me_4PNP^{iPr}** is a viscous jelly that is unstable in air, while **Me_4PNP^{tBu}** is a crystalline solid. Both protected forms are crystalline and can be kept for months under air without degradation. The deprotected ligands can be reacted *in situ*, in one pot after the deprotection step, with anhydrous Ni^{II} dihalides in THF at 60 °C overnight to afford complexes [Me_4PNP^{iPr}NiBr]Br (**[1]Br**), [Me_4PNP^{iPr}NiCl]Cl (**[2]Cl**), [Me_4PNP^{tBu}NiBr]Br (**[3]Br**), and [Me_4PNP^{tBu}NiCl]Cl (**[4]Cl**) in 57% to 85% yield. The halide counter-ion can be replaced using sodium tetrakis[3,5-bis(trifluoromethyl)phenyl]borate ($NaB(Ar^F)_4$) to afford complexes **[1]B(Ar^F)$_4$**, **[2]B(Ar^F)$_4$**, **[3]B(Ar^F)$_4$**, and **[4]B(Ar^F)$_4$** in 67% to quantitative yield (See Scheme 2). Those complexes allow for facile characterization by electrochemical methods.

^{1}H NMR spectra of bis(isopropyl)phosphine-based complexes **[1]X** and **[2]X** (X = Br, Cl, or $B(Ar^F)_4$) exhibit two overlapping doublets corresponding to Me groups of the CMe_2 arms with splitting to the phosphorus atom, suggesting a lack of a mirror plane through the coordination plane of the square planar Ni complexes. This is also consistent with their solid-state structures (vide infra). Methyl groups of ^{i}Pr groups also appear as two sets of multiplets showing splitting to the phosphorus atom. Complexes with bis(*tert*-butyl)phosphine donors show broadened signals for ^{t}Bu groups and Me groups of the ligand arm in ^{1}H NMR spectrum due to hindered rotation. VT NMR study of complex **[3]B(Ar^F)$_4$** reveals that a broadened signal of one of the ^{t}Bu groups resolves into three separate signals of Me groups, while the other broad singlet of ^{t}Bu group remains unresolved even at –60 °C (see Figure S76).

Solid-state structures of Ni^{II} complexes. All the complexes shown in Scheme 2 were analyzed by X-ray diffraction after their crystals were grown by different methods using either THF, acetone or benzene at rt or -30 °C. Table 1 lists the Ni-ligand bond lengths and Ni centered bond angles for complexes **[1]-[4]**, showing almost ideal square planar geometry around the metal center for this series of Ni^{II} complexes. The ORTEP diagrams of complexes **[1]X-[4]X** (X= Cl, Br) are presented in Figure 1, while those of complexes **[1]B(Ar^F)$_4$-[4]B(Ar^F)$_4$** are presented in Figures S5 to S8 of the SI.

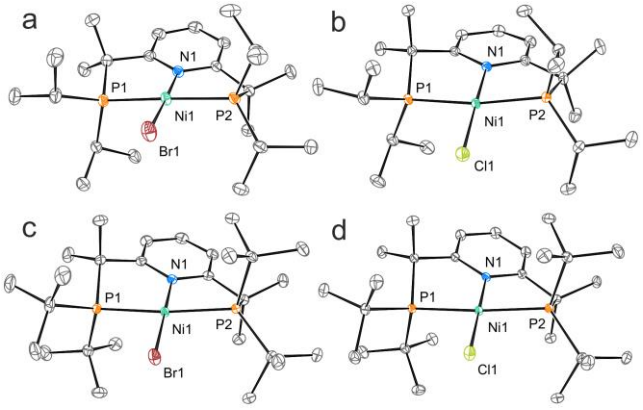

Figure 1. ORTEP diagrams for the cationic parts of complexes **[1]Br** (a), **[2]Cl** (b), **[3]Br** (c), and **[4]Cl** (d) with the thermal ellipsoids set at 50% probability level. Hydrogen atoms, counterions and solvent molecules are omitted for clarity.

Table 1. Bond distances [Å] and angles [deg] for complexes [1]-[4]. The atom numbering corresponds to that of Figure 1.

Complex	Ni1–N1	Ni1–Hal	Ni1–P1	Ni1–P2	∠ P1–Ni1–P2	∠ N1–Ni1–Hal	τ_4'[a]	τ_4
[1]Br	1.918(2)	2.3015(4)	2.1880(6)	2.1924(6)	171.36(3)	176.49(6)	0.07	0.09
[2]Cl	1.9153(7)	2.1658(2)	2.1922(2)	2.1861(2)	171.336(10)	176.52(2)	0.07	0.09
[3]Br	1.9222(19)	2.3070(3)	2.2394(6)	2.2413(6)	171.68(2)	179.45(6)	0.04	0.06
[4]Cl	1.9166(8)	2.1643(3)	2.2220(3)	2.2201(3)	171.405(11)	179.51(3)	0.04	0.06
[1]B(Ar^F)$_4$[b]	1.9095(13)	2.2827(2)	2.1786(4)	2.1805(4)	172.320(18)	176.66(4)	0.06	0.08
[2]B(Ar^F)$_4$[b]	1.9135(11)	2.1548(3)	2.1763(3)	2.1779(3)	173.359(14)	179.34(3)	0.03	0.05
[3]B(Ar^F)$_4$[c]	1.9236(15)	2.2877(12)	2.2324(12)	2.2454(13)	171.87(5)	178.84(7)	0.04	0.07
[4]B(Ar^F)$_4$	1.9119(9)	2.1531(3)	2.2333(3)	2.2275(3)	172.587(12)	179.29(3)	0.04	0.06

[a] Geometrical index τ_4' and τ_4 for the nickel centers is calculated according to refs. [99-101]. [b] There are two complexes in the asymmetric unit; data are tabulated for the first one. [c] Data are listed for the main disordered component.

.

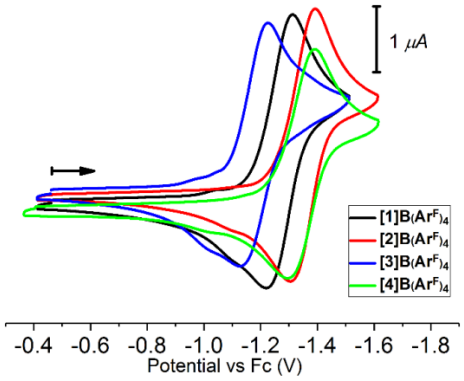

Figure 2. Cyclic voltammogram of complexes **[1]B(Ar^F)$_4$** to **[4]B(Ar^F)$_4$** (1 mM) in 0.1 M ^{n}Bu$_4$NPF$_6$/MeCN solution at 23 °C (scan rate 0.1 V s^{-1}; 1.0 mm GC disk working electrode; the arrow indicates the initial scan direction).

Table 2. Electrochemical properties of complexes [1]B(Ar^F)$_4$ to [4]B(Ar^F)$_4$ (V vs. Fc)

Complex	$E_{1/2}$ for $Ni^{II/I}$ vs. Fc[a] (ΔE_p)[b]
[1]B(Ar^F)$_4$	–1.27 V (94 mV)
[2]B(Ar^F)$_4$	–1.35 V (90 mV)
[3]B(Ar^F)$_4$	–1.17 V (99 mV)
[4]B(Ar^F)$_4$	–1.34 V (95 mV)

[a] Measured vs. Fc^+/Fc by CV in 0.1 M ^{n}Bu$_4$NPF$_6$/MeCN, scan rate 100 mV s^{-1}. [b] ΔE_p is the peak potential separation calculated as difference between forward and reverse peak potentials.

The geometry index for 4-coordinate complexes, τ_4', varies between 0.03 and 0.07, which is close to the ideal square planar value of τ_4' = 0.[101] Complexes **[1]** to **[4]** show insignificant variation in the Ni–N_{py} bond lengths (1.9034(11) to 1.9236(15) Å) and the Ni-halogen bond length varies only slightly between the same halogen-containing complexes (2.2827(2) to 2.3070(3) Å for Br, 2.1462(3) to 2.1658(2) Å for Cl-containing complexes).

Electrochemical properties of Ni^{II} complexes. To test the stability of the bulky PNP framework and the possibility of oxidation or reduction of its associated nickel complexes, we studied the redox properties of the BH_3 protected ligand and Ni^{II} complexes with [B(Ar^F)$_4$] counterion using cyclic voltammetry in MeCN solution using ^{n}Bu$_4$NPF$_6$ as an electrolyte. (See Figures S102 to S107 in Supporting Information for the full voltammograms of all complexes and ligands).

The protected ligands show two irreversible oxidation peaks in acetonitrile (See Table S9 in Supporting Information). For **Me$_4$PNP^{iPr}BH$_3$**, the first oxidation appears at 0.92V and the second at 1.78 V, while **Me$_4$PNP^{tBu}BH$_3$** has oxidation potentials at 1.16 V and 1.87 V. No reduction waves are observed to -2.5 V vs. Fc for both ligands The complexes **[1]B(Ar^F)$_4$** to **[4]B(Ar^F)$_4$** exhibit quasi-reversible reduction waves (See Figure 2 and Table 2) with redox potentials ranging from -1.17 to -1.35 V vs. Fc and a peak-to-peak separation between 90-99 mV. We assign this wave to the $Ni^{II/I}$ reduction, which is confirmed by further studies (vide infra). Generally, the $Ni^{II/I}$ reduction potentials $E_{1/2}$ of complexes containing a chloride, such as **[2]B(Ar^F)$_4$** ($E_{1/2}$ = -1.35 V) or **[4]B(Ar^F)$_4$** ($E_{1/2}$ = -1.34 V),

Scheme 3. Preparation of neutral Ni^I complexes 5-8 via electrochemical or chemical reduction with cobaltocene

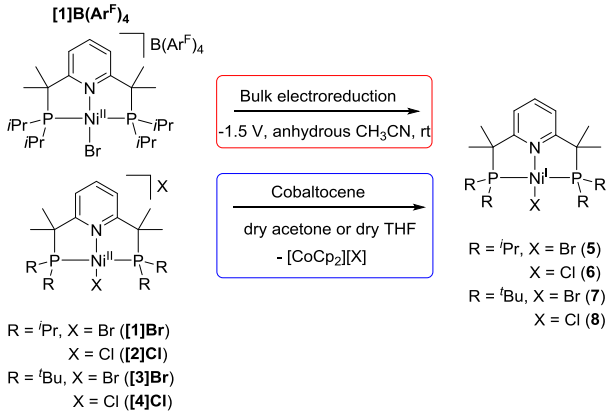

Table 3. Selected EPR parameters[a] and effective magnetic moment μ_{eff} in solution for Ni^{I} complexes.

Complex	g_x, g_y, g_z[b]	g_{iso}	A_{xx} (G)[b]	A_{yy} (G)[b]	A_{zz} (G)[b]	μ_{eff} (μ_B)[c]
5	2.316, 2.309, 1.993	2.206	n.d.	n.d.	n.d.	2.07
6	2.355, 2.293, 1.990	2.213	n.d.	n.d.	A^{P}_{zz} = 18.7; A^{N}_{zz} = 9.34	2.18
7	2.240, 2.150, 1.983	2.124	A^{Br}_{xx} = 57.5; A^{P}_{xx} = 49.8; A^{N}_{xx} = 7.77.	A^{Br}_{yy} = 60.4; A^{P}_{yy} = 51.8; A^{N}_{yy} = 8.48.	A^{Br}_{zz} = 62.3; A^{P}_{zz} = 55.6; A^{N}_{zz} = 9.31.	1.94
8	2.250, 2.120, 2.000	2.123	A^{Cl}_{xx} = 10.7; A^{P}_{xx} = 44.5; A^{N}_{xx} = 7.56.	A^{Cl}_{yy} = 11.3; A^{P}_{yy} = 67.4; A^{N}_{yy} = 8.02.	A^{Cl}_{zz} = 12.0; A^{P}_{zz} = 71.4; A^{N}_{zz} = 8.50.	1.82

[a]MeTHF/acetone glass or frozen acetone, 84-95 K. [b]From simulated spectra. For complex **6**, simulation cannot provide reliable superhyperfine splitting constants for g_x and g_y components due to signal broadening. [c]Evans method, acetone-d_6 solvent, 298 K.

are more negative than those of complexes containing a bromide ligand, such as **[1]B(Ar^F)$_4$** ($E_{1/2}$ = -1.27 V) and **[3]B(Ar^F)$_4$** ($E_{1/2}$ = -1.17 V). All complexes also show irreversible oxidation waves around 0.93 to 1.45 V. However, considering that the protected ligands also feature an irreversible oxidation wave at 0.98 V and 1.16 V vs. Fc for the **Me$_4$PNP^{iPr}BH$_3$** and **Me$_4$PNP^{tBu}BH$_3$**, respectively, it likely corresponds to ligand oxidation. Accordingly, attempted detection of Ni^{III} intermediates by EPR spectroscopy during one-electron electrochemical or chemical oxidation of complex **[1]B(Ar^F)$_4$** did not lead to any detectable paramagnetic species, and no single product could be isolated.

Coulometric study of the reduction of complex **[1]B(Ar^F)$_4$** confirmed that the reduction wave corresponds to a one-electron process (See Supporting Information Figure S108 for experimental details). Such reversible reduction waves suggested that stabilization of the uncommon Ni^{I} oxidation state might be possible and led us to further investigate one-electron reduction chemistry of Me$_4$PNP nickel halide complexes. A second irreversible reduction wave is observed at around -2.0 V for all complexes, which likely corresponds to the $Ni^{I/0}$ reduction (see Supp. Info for more detail).

Synthesis of Ni^{I} complexes and their characterization in solution. Following the cyclic voltammetry analysis, we performed bulk electrolysis of a 1 mM solution of **[1]B(Ar^F)$_4$** in anhydrous acetonitrile, which led to a gradual change of the solution color from orange to dark brown. An aliquot of the solution obtained via electroreduction of **[1]B(Ar^F)$_4$** was analyzed by EPR spectroscopy (See Figure 3a, dashed lines), which showed a nearly axial signal with g-values significantly deviating from 2 (vide infra), suggesting significant metal-centered radical character (See Supporting Information for details).

In order to isolate the reduction product in pure form, we attempted chemical reduction of complex **[1]Br** with 1 equivalent of cobaltocene in dry acetone solution at room temperature. Gratifyingly, chemical reduction led to the formation of a dark-red solution, from which crystalline product **5** was isolated in 79% yield. The EPR spectrum of crystalline **5** re-dissolved in acetone was essentially identical to that obtained by electrochemical reduction (see Figure 3a, solid lines).

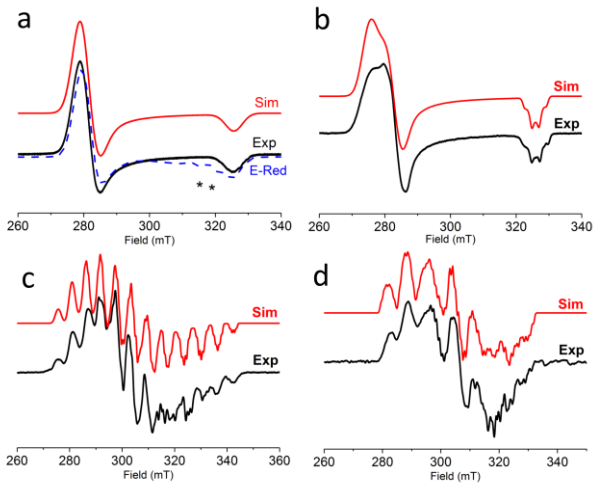

Figure 3. Experimental (black line) and simulated (red line) EPR spectra of Ni^{I} complexes: (a) isolated complex **5** in frozen acetone, 80K (solid line) and the product of electroreduction of **[1]B(Ar^F)$_4$** (dashed blue line), frozen MeCN, 83.5K; (b) isolated complex **6**, MeTHF glass, 92K; (c) isolated complex **7**, 20% acetone/80% MeTHF/acetone glass, 95K; (d) isolated complex **8**, MeTHF/acetone glass, 95K. See Table 3 and Table S1 in SI for simulated and experimental parameters, respectively.

In a similar way, chemical reduction of complexes **[2]Cl**, **[3]Br**, and **[4]Cl** with cobaltocene in dry acetone at room temperature led to the formation of complexes **6**, **7**, and **8**, which were isolated as crystalline samples in 65-85% yields by slow evaporation of concentrated acetone solution at -30°C. The complexes were characterized by UV-vis, FT-IR, EPR, UV-vis and X-ray diffraction (vide infra).

The EPR spectrum of isolated bromo-complex **5** reveals a rhombic signal with g_x and g_y values that are close to each other, and without discernible superhyperfine splitting due to signal broadening. This signal broadening might be due to unresolved splitting from Br and P nuclei similar to other reported Ni^{I} complexes.[57] By comparison, EPR spectra of an analogous chloro-complex **6** shows a rhombic signal (Figure 3 b), with g_x = 2.355; g_y = 2.293 and g_z = 1.990. Superhyperfine splitting was observed for g_z component, which could be simulated as splitting from two phosphorus atoms.

Table 4. Selected bond distances [Å] and angles [deg] for complexes 5 to 8

Complex	Ni1–N1	Ni1–Hal	Ni1–P1	Ni1–P2	∠ P1–Ni1–P2	∠ N1–Ni1–Hal	τ_4'	τ_4
5	1.9821(10)	2.48133(19)	2.2030(3)	2.1952(3)	149.357(13)	109.65(3)	0.59	0.72
6[a]	1.9833(9)	2.3414(3)	2.2066(3)	2.1976(3)	148.029(13)	110.76(3)	0.60	0.72
7	2.0973(9)	2.51129(18)	2.3021(3)	2.3024(3)	161.830(12)	173.54(3)	0.14	0.17
8	2.1176(7)	2.3723(2)	2.2943(2)	2.2960(2)	161.509(9)	173.88(2)	0.14	0.17

[a] The bond distances and angles are those of the major disordered component.

and one nitrogen donor, with superhyperfine splitting constants of 18.7 G and 9.34 G, respectively

Interestingly, ^{t}Bu substituted complexes **7** and **8** feature a more complex EPR signal pattern, which shows distinct splitting from the pincer ligand donor atoms as well as the halogen. The spectra could be simulated as rhombic signals showing splitting from nitrogen and two phosphorus atoms and with a contribution from bromide for complex **7** or chloride for complex **8** (Figure 3 c). The g-values and superhyperfine splitting constants for complexes **5-8** are summarized in Table 3. In all cases, EPR spectroscopy confirms an S = ½ spin state for complexes **5-8**, while g_{iso} values (2.123-2.213) suggest metalloradical character, consistent with our DFT studies (vide infra).

The magnetic moment of complexes **5-8** in acetone solution was measured using the Evans method at RT (see Table 3). The value for μ_{eff} was found to be in a range from 1.82 to 2.18 μ_B, consistent with a d^9 configuration.

Solid-state structures of Ni^I complexes. The different EPR signal symmetry and splitting patterns in the case of ^{t}Bu and ^{i}Pr substituted complexes suggested that the geometry around the metal center might also show significant differences depending on the steric environment of the phosphine donors. We were able to grow single crystals of Ni^I complexes, **5** and **6** (red crystals), **7** (dark orange), and **8** (dark red crystals), which were analyzed by X-ray diffraction. Analysis of the crystal structures confirmed that complexes **5-6** and **7-8** have very different geometry around the metal center that were consistent with their different EPR spectral patterns. As shown in Figure 4 and Table 4, Ni^I complexes containing ^{i}Pr groups on the phosphine donor have a very unusual see-saw-like geometry (τ_4'= 0.59 and 0.60 for **5** and **6**, respectively) with the halide ligand present above the plane formed by the Ni atom with PNP pincer ligand. Thus, N_{py}–Ni–Hal (Hal = Br, Cl) angles for **5** and **6** were found to be 109.65(3) and 110.76(3), respectively. Coordination of the Me_4PNP^{iPr} is not planar and shows P1-Ni1-P2 angles of 149.357(13) and 148.029(13) for complexes **5** and **6**, respectively. By contrast, ^{t}Bu substituted complexes **7** and **8** display a distorted square planar geometry (τ_4'= 0.14) with the halide present *trans* to pyridine and N_{py}–Ni–Hal (X = Br, Cl) angles of 173.54(3) and 173.88(2), respectively.

All the Ni^I complexes show elongation of the Ni–Hal bond compared to the corresponding Ni^{II} precursors. Ni^I bromide complexes **5** and **7** have Ni1–Br1 bond lengths 0.17 and 0.20 Å longer than their Ni^{II} bromo analogues **[1]Br** and **[3]Br**.

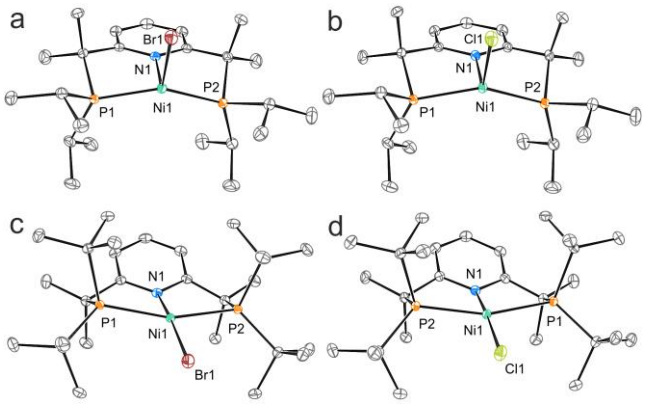

Figure 4. ORTEP diagrams of complexes **5** (a), **6** (b), **7** (c), and **8** (d) with the thermal ellipsoids set at 50% probability level. Hydrogen atoms, solvent molecules and a minor disordered component for **6** are omitted for clarity.

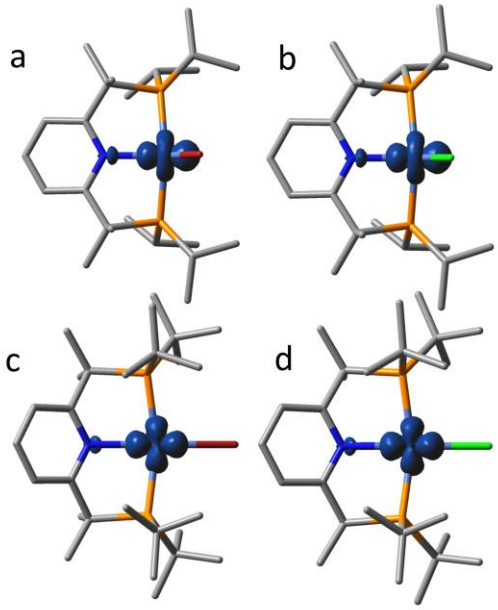

Figure 5. Mulliken atomic spin density plots of **5** (a), **6** (b), **7** (c), and **8** (d) (DFT-optimized geometries, B3LYP, lanl2dz/6-311++G**). (a) Ni 88.8%, Br 1.2%, P 1.7%, N 3.4%; (b) Ni 87.9%, Cl 1.2%, P 2.4%, N 3.4%; (c) Ni 86.8%, Br 4.1%, P 0.9%, N 1.8%; (d) Ni 85.2%, Cl 3.8%, P 1.8%, N 1.4%.

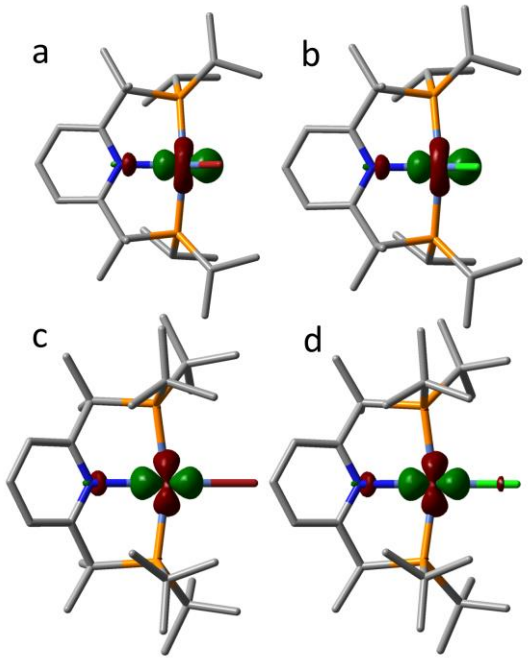

Figure 6. The SOMO representation of **5** (a), **6** (b), **7** (c), and **8** (d) (DFT-optimized geometries, B3LYP, lanl2dz/6-311++G**)).

The same trend is repeated in chloro-containing complexes **6** and **8** with respect to **[2]Cl** and **[4]Cl**. No significant differences in the ligand C-C or C-P bond lengths are present between the complexes **[1]Br** to **[4]Cl** and **5** to **8**, giving credence to the initial vision of designing the ligand system with a view to limit ligand-centered reactivity.

Computational analysis of the Ni^{I} complexes. The metalloradical nature of the Ni^{I} complexes was further confirmed by DFT studies, which showed that the spin density is mainly localized on the metal. Figure 5 shows the Mulliken atomic spin density plot for the optimized geometries for complexes **5**-**8**, with 85-89% of spin density present at the Ni center, consistent with a d^{9} configuration. At the same time, slightly higher Mulliken spin density at the halogen atoms was found for square-planar complexes **7** and **8** than in bent complexes **5** and **6**.

The Natural Population Analysis (NPA), Mulliken population and LCAO-MO analyses reveal that the SOMO has essentially a $d_{x^2-y^2}$ character in all the complexes (Figure 6 and Supporting Information, Tables S11 and S14), which resembles the Ni^{I} complexes reported by Lee and Gade. [65,92] In combination with higher calculated spin density at the halogen atoms, this is also in accordance with more pronounced superhyperfine splitting from halogens observed in EPR spectra of square planar complexes **7** and **8** compared to bent complexes **5** and **6**. In Lee's case, T-shaped complexes could be obtained for Ni complexes bearing anionic PNP ligands having a central amide donor, where no ligands were present in *trans* position to that amide. Addition of CO or PMe_3 to their complexes lead to the formation of complexes where the CO or PMe_3 ligands deviate from the (PNP)Ni plane.

Such deviations helped to diminish the antibonding interactions of the SOMO, which has the character of a singly-occupied $d_{x^2-y^2}$ orbital.[92] Similarly, the formation of bent geometries in **5** and **6** by bending of the N_{Py}–Ni–Hal (Hal = Br, Cl) plane and the elongation of Ni–Hal bond might be driven by the minimization of antibonding interactions in our system.

Energy minimization of square planar ^{i}Pr complexes **5** and **6** led to an energy minimum where the bent structure was obtained, while the geometry of the more sterically hindered ^{t}Bu complexes **7** and **8** remained square planar after optimization of the structures where the halide ligand was forced into the bent position. This is likely due to the steric clash between the bulky ^{t}Bu groups and Me groups on the phosphine and ligand arm, respectively, which prevents the formation of the bent structure.

Table 5. Exact ligand solid angle and ligand shielding parameters from the DFT-optimized geometry Ni^{I} complexes with[a] and without the halogen[b]

Entry	Complex	Exact solid angles Ω°/ str [c]	G[d] % [c]
1	**5**	10.34 (10.89)	82.3 (86.7)
2	**5** w/out Br	8.43 (9.09)	67.1 (72.4)
3	**6**	10.09 (10.92)	80.3 (86.9)
4	**6** w/out Cl	8.50 (9.18)	67.7 (73.1)
5	**7**	10.65 (11.31)	84.7 (90.0)
6	**7** w/out Br	8.98 (9.77)	71.4 (77.8)
7	**8**	10.52 (11.38)	83.7 (90.6)
8	**8** w/out Cl	9.09 (9.90)	72.3 (78.7)

[a]Calculated for DFT-optimized structures, B3LYP, lanl2dz/6-311++G**. [b]Calculated for fragments of DFT-optimized structures with halide atom artificially removed; after removing halogen, no further geometry optimization was carried out. [c]The values in parenthesis were calculated using the Bondi radii for all atoms,[102] while the values outside the parentheses were calculated using the zero energy point radii.[103] [d]Ligand shielding parameter.

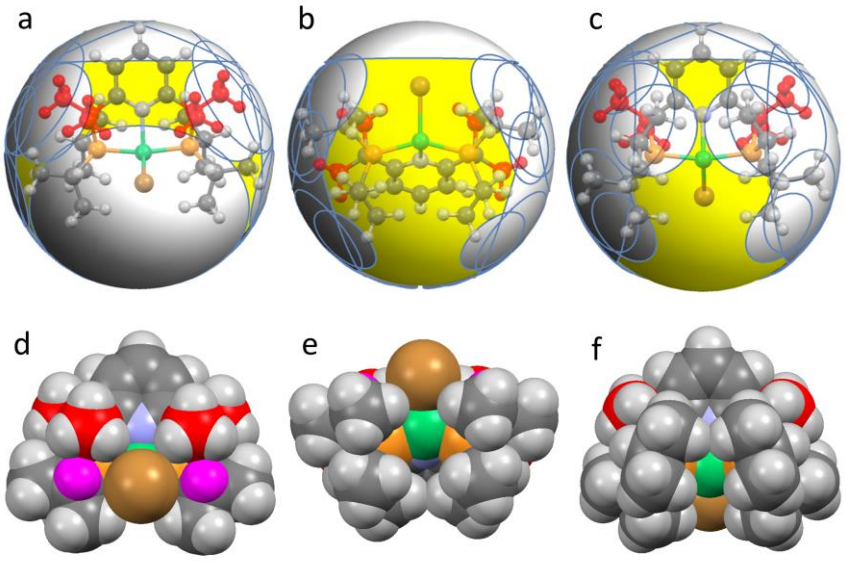

Figure 7. Selected ligand solid angle representations (grey area) of the optimized structure of **5** (a-c). Corresponding space filling model representation of the optimized structure of **5** (d-f). Nickel atom is represented in green, phosphorous atoms in light orange, bromide atom in light brown. Atoms highlighted in red are the methyl groups on the ligand arms; the isopropyl C-H hydrogen is highlighted in magenta. Zero energy radii were used for computation.

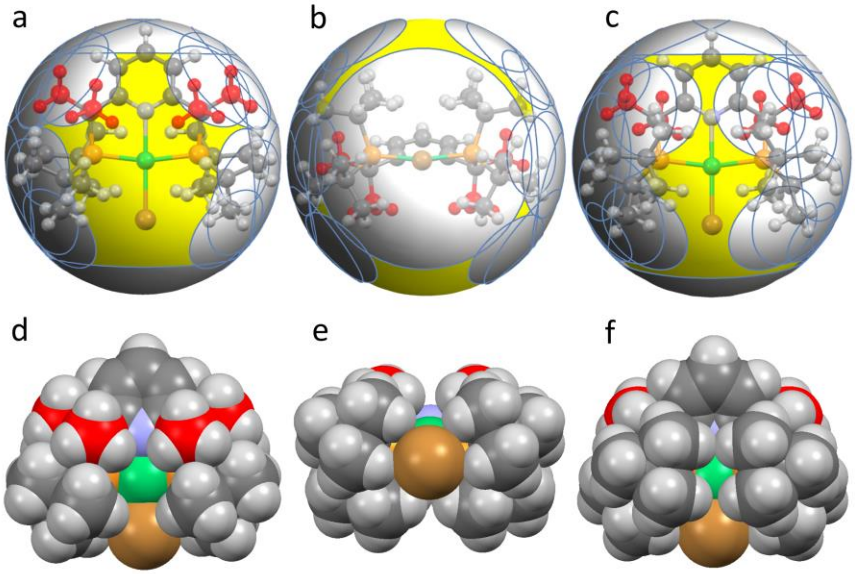

Figure 8. Selected ligand solid angle representations (grey area) of the optimized structure of **7** (a-c). Corresponding space filling model representation of the optimized structure of **7** (d-f). Nickel atom is represented in green, phosphorous atoms in light orange, bromide atom in light brown.

To rationalize and as alternative to visualize that the Ni-halogen bond is out of the plane in ^{i}Pr-containing complexes, we calculated the exact solid angles of the DFT-optimized geometries of Ni^{I} complexes, the solid-state complexes, as well as their fragments from which halogen was removed (to better visualize the area occupied by the halogen, see Supporting Information). As an alternative to the Tolman cone angle, especially for rotationally hindered or highly asymmetric ligands, the exact ligand solid angle (Ω°) should be able to describe the steric hindrance of our ligand system in a quantitative and visual manner. Moreover, we can calculate an easily interpretable parameter (G) that describes ligand shielding as a simple percentage of the maximum solid angle of 4π steradians (G = 100Ω°/4π), which is described and advocated both by Guzei and Wendt,[103] as well as by Allen.[104] The results of the exact solid angle (Ω°) calculations and of the ligand shielding parameter (G) are reported in Table 5. An overlay of a ball-and-stick representation of the calculated geometry, or of the experimental X-ray coordinates on the sphere created by the exact ligand solid angle method are shown in Figures 7 and 8, and Figure S121 to S156 in the Supporting Information.

The ^{i}Pr-containing complexes **5** and **6** have exact solid angles of 10.34 and 10.09, which correspond to a ligand shielding (G) of 82.3 and 80.3 % for DFT-optimized structures. In contrast,

both the ^{t}Bu containing complexes **7** and **8** have higher exact solid angles (Ω°) of 10.65 and 10.52, which corresponds to higher ligand shielding of 84.7 and 83.7%, respectively.

Although the exact ligand angles or the ligand shielding parameter by itself might seem to show only a small difference between ^{i}Pr and ^{t}Bu containing complexes, it is a useful way to visualize the voids available in the complexes, alternative to space filling models (Figure 7). For example, comparison of the solid angle representation of complexes **5** and **6** shows that while for the bis(*iso*-propyl)phoshine-substituted **5**, the void is available to bind Br in the position bent from the plane of (PNP)Ni fragment, such binding would not be possible for bis(*tert*-butyl)phoshine-substituted **6** due to steric clash between Me groups of the CMe_2 arm (shown in red) and *tert*-butyl groups on the phosphines.

To estimate the steric requirements of the new bulky PNP ligands in these complexes, we also compared exact solid angles for both ligands with ^{i}Pr and ^{t}Bu substituents by calculating Ω and G parameters for a hypothetical **(Me$_4$PNP^R)Ni** (R = ^{t}Bu, ^{i}Pr) fragment where halide was removed from DFT-optimized structures (Table 5, entries 2, 4, 6, and 8). These parameters can be used as approximate estimates applicable to the system under consideration as not all possible conformers of the ligands were considered. This gives G values of 67.1-67.7% for ^{i}Pr-substituted ligand and expectedly larger values, 77.8-78.7%, for ^{t}Bu-substituted ligand, meaning that these new bulky ligands occupy as much as ca. 67-79% of the total unit sphere.

Overall, this analysis shows that not only steric parameters of ^{t}Bu- and ^{i}Pr-substituted ligands are different, but also greater steric hindrance of the ^{t}Bu-substituted ligand likely makes the bent position above the coordination plane of the (PNP)Ni fragment unavailable to binding an additional ligand, leading to an enforced square planar coordination.

SUMMARY AND CONCLUSION

By designing a ligand that is both bulky and blocks possible MLC via dearomatization on the pincer arm, we were able to stabilize and fully characterize reactive Ni^I species, which are usually difficult to isolate. We first investigated the redox properties of the Ni^{II} complexes and found that the reduction of Ni^{II} to Ni^I is both reversible and easily accessible by reductants such as cobaltocene. We also investigated the EPR spectra of each Ni^I species and found that both their shape, g-values and hyperfine coupling constants vary significantly when changing from the less bulky ^{i}Pr complexes **5** and **6** to the bulkier ^{t}Bu complexes **7** and **8**. Solid-state structural analysis revealed that the geometry around the metal center is completely different for **5** and **6** (see-saw) and **7** and **8** (distorted square planar). Spin density and orbital analysis of the complexes has shown that all complexes are essentially metalloradicals with the SOMO that has mostly a $d_{x^2-y^2}$ character, similar to previously reported Ni^I complexes with anionic PNP ligands. Interestingly, having bulkier ^{t}Bu substituents on the phosphine donors results in a dramatic geometry difference for the reduced Ni^I complexes; with calculations of steric environment around the complex showing that this difference, which is reflected in EPR spectra, is brought about by steric and not electronic effects.

Overall, introducing new bulky PNP pincer ligands may open new possibilities for studying one-electron redox-transformations of late 1st row transition metals by providing steric protection and disabling metal-ligand cooperative reactivity, as we have shown for the Ni^I test case. Additional steric hindrance introduced by four methyl groups at the pincer ligand arm also creates new modes of controlling coordination geometry of the metal center. Utilizing these 'innocent' ligands may enable for the tuning of desired reactivity by varying steric (and/or electronic) parameters in a systematic manner, without turning on undesired side-reactivity. Further studies will focus on studying the reactivity and catalytic activity of organometallic late transition metal complexes coordinated by these new, bulky PNP ligands.

EXPERIMENTAL SECTION

Unless otherwise indicated, all solvents and reagents were used as received. Non-deuterated solvents were taken from a solvent purification system (MBRAUN SPS). Acetone-d_6 was vacuum distilled over dried magnesium sulfate at low temperature. All other deuterated solvents were added to activated 3 Å molecular sieves. Di-*iso*-propylchlorophosphine, di-*tert*-butylchlorophosphine, nickel(II) chloride anhydrous, and cobaltocene were purchased from Sigma-Aldrich; BH_3-THF and nickel(II) bromide 99% were purchased from Acros Organics; ^{n}butyl lithium, 2,6-bis(chloromethyl)pyridine was purchased from Kanto Chemical Co., Inc. The reported yields are based on isolated solids. NMR spectra were recorded using JEOL ECZR-400 MHz or ECZR-600 MHz. Chemical shifts are reported in ppm (δ) and referenced internally to the residual solvent signals (^{1}H and ^{13}C: 7.26 and 77.16 ppm for $CDCl_3$; 2.05 and 29.84, 206.26 ppm for acetone-d_6; 1.94 and 1.32, 118.26 ppm for CD_3CN). The signal abbreviation is as follows: d – doublet, t – triplet, v – virtual, q – quartet, br - broad, m – multiplet. X-band EPR spectra were recorded on an X-band JEOL JES-X330 instrument using liquid nitrogen-cooled cryostat in 5 mm diameter quartz tubes. Fourier transform infrared (FT-IR) spectra were recorded for crystalline samples under an Ar atmosphere on a Cary 630 with an attenuated-total-reflectance (ATR) module. Electrochemical grade tetrabutylammonium hexafluorophosphate (^{n}Bu$_4$NPF$_6$) from Sigma-Aldrich was used as the supporting electrolyte. Cyclic voltammetry and control potential electrolysis experiments were performed on an ALS CHI 660E electrochemical workstation. The electrochemical measurements were done under an N_2 atmosphere. Acetonitrile used for the solutions was dried by the MBRAUN SPS solvent system. A glassy carbon disk electrode (d = 1.0 mm) or a Pt gauze were used as working electrodes for cyclic voltammetry and for controlled potential electrolysis, respectively. A non-aqueous Ag-wire reference electrode assembly was filled with 0.01M $AgNO_3$ in 0.1 M ^{n}Bu$_4$NPF$_6$/MeCN solution as a reference electrode. A Pt-wire or a Pt gauze were used as an auxiliary electrode for cyclic voltammetry and for the controlled potential electrolysis experiments, respectively. The reference electrodes were calibrated against $FeCp_2$ (Fc), where the Fc/Fc$^+$ couple vs Ag/$AgNO_3$/MeCN non-aqueous reference is 102 V in 0.1 M ^{n}Bu$_4$NPF$_6$/MeCN. The preparation of PH^{t}Bu$_2$-BH_3 and PH^{i}Pr$_2$-BH_3 were reported elsewhere.[105,106]

The X-ray diffraction data for the single crystals was collected on a Rigaku XtaLab PRO instrument (an ω-scan mode) with a PILATUS3 R 200K hybrid pixel array detector and a MicroMax^{TM}-003 microfocus X-ray tube using Mo*Kα* (0.71073 Å) radiation at low temperature. Images were indexed and integrated using the *CrysAlis*^{Pro} data reduction package. Data were corrected for systematic errors and absorption using the *ABSPACK* module: Numerical absorption correction based on Gaussian integration over a multifaceted crystal model and

empirical absorption correction based on spherical harmonics according to the point group symmetry using equivalent reflections. The *GRAL* module was used for analysis of systematic absences and space group determination. The structures were solved by direct methods using *SHELXT*[107] and refined by the full-matrix least-squares on F^2 using *SHELXL*.[108] Non-hydrogen atoms were refined anisotropically. The hydrogen atoms were inserted at the calculated positions and refined as riding atoms. The positions of the hydrogen atoms of methyl groups were found using rotating group refinement with idealized tetrahedral angles. The disorder, if present, was resolved using free variables and reasonable restraints on geometry and anisotropic displacement parameters.

2,6-bis(di-*tert*-butylphosphinomethyl)pyridine, boron trihydride adduct, PNP^{tBu}BH$_3$. Although this ligand was previously reported,[109] an alternative procedure was used to give the desired product that does not require further purification. In a flame-dried 500 mL round-bottom flask under Ar the previously synthesized precursor PH^{t}Bu$_2$-BH$_3$ was added, (10.00 g, 62.48 mmol, 2.22 eq.) followed by 200 mL of dry THF, after which the temperature was lowered to 0 °C. After 10 minutes of stirring a 2.6 M solution of n-butyl lithium (26.24 mL, 68.66 mmol, 2.44 eq.) was added. The reaction was stirred for 3 hours at room temperature, and 2,6-bis(chloromethyl)pyridine (4.955 g, 28.14 mmol, 1.00 eq.) was added. The reaction was allowed to reach room temperature and left to stir overnight. Water was added to quench the reaction and the aqueous phase was extracted with 3 portions of 150 mL of diethyl ether. The combined organic phases were washed with a saturated sodium hydrogen carbonate solution, then with a saturated brine solution. The organic phases were combined, dried over magnesium sulfate, filtered and evaporated under reduced pressure to afford a white crystalline solid, that was washed several times with a minimum amount of hexane to afford the pure product (11.83 g, 87.7 %). Crystals suitable for X-ray analysis were obtained by slow evaporation of THF at room temperature.

[2,6-bis(2-di-*tert*-butylphosphino-2-propyl)pyridine boron trihydride adduct, Me$_4$PNP^{tBu}BH$_3$. PNP^{tBu}BH$_3$ (1.00 g, 2.36 mmol, 1.00 eq.) was added into a dry 250 mL round-bottom flask under Ar, to which was later added 100 mL of dry THF and the entire solution was then cooled to 0 °C with an ice bath. Then, successively and with 2 minutes between each addition, a 2.6 M solution of n-butyl lithium (0.91mL, 2.36 mmol, 1.00 eq.) was slowly added, followed by iodomethane (147 µL, 2.36 mmol, 1.00 eq.) for a total of 6 additions of both reagents. The reaction was further stirred at room temperature for 10 minutes and was quenched with 50 mL of water. The aqueous phase was separated and washed with 3 portions ethyl acetate (note: washing with diethyl ether gives similar yields if the extraction is done quickly). The organic phases were then washed with a saturated solution of sodium hydrogen carbonate followed by a saturated brine solution. The organic phases were combined, dried over magnesium sulfate, filtered, and concentrated under reduced pressure. The resulting slightly off-white solid was washed 3 times with a minimal amount of hexanes (1-2 mL) and the liquid was carefully decanted using a Pasteur pipet. The solid was then dried again under reduced pressure to afford a white solid (0.96 g, 85%). ^{1}H NMR (600 MHz, $CDCl_3$) δ 0.41-0.71 (br m, 6H, P-B$\underline{\boldsymbol{H_3}}$), 1.05-1.48 (br m, 36H, Me of ^{t}Bu), 1.92 (br s, 12H, PC-(C$\underline{\boldsymbol{H_3}}$)$_2C_{py}$), 7.57 (t, J_{HH} = 8.0 Hz, 1H, C$_{py}$-$\underline{\boldsymbol{H}_{para}}$), 7.90 (d, J_{HH} = 8.0 Hz, 2H, C$_{py}$-$\underline{\boldsymbol{H}_{meta}}$). ^{13}C{^{1}H} NMR (151 MHz, $CDCl_3$) δ 28.46 (d, J_{PC} = 36.6 Hz, C$_{quat}$ of ^{t}Bu), 30.24 (br, Me of ^{t}Bu), 36.91 (d, J_{PC} = 19.5 Hz, P-$\underline{\boldsymbol{C}}$(CH$_3$)$_2C_{py}$), 45.68 (d, J_{PC} = 14.7 Hz, PC-($\underline{\boldsymbol{C}}H_3$)$_2C_{py}$), 125.16 ($\underline{\boldsymbol{C}_{py,meta}}$), 135.59 ($\underline{\boldsymbol{C}_{py,para}}$), 161.19 ($\underline{\boldsymbol{C}_{py,ortho}}$). ^{31}P{^{1}H} NMR (162 MHz, $CDCl_3$) δ 63.99, 63.66. UV-vis (CH_2Cl_2, [1·10^{-4} M]), λ_{max}, nm (ε, L·mol^{-1}·cm^{-1}): 263 (10500), 269 (12100), 276 (10000). Anal. Calcd. For $C_{27}H_{57}B_2NP_2$: C, 67.66; H, 12.06; N, 2.92. Found: C, 67.59; H, 12.01; N, 3.20.

2,6-bis(di-isopropylphosphinomethyl)pyridine, boron trihydride adduct, PNP^{iPr}BH$_3$. The analogous procedure to prepare **PNP^{tBu}BH$_3$ ligand** was used to prepare **PNP^{iPr}-BH$_3$** ligand. PH^{i}Pr$_2$-BH$_3$ (10.0 g, 76.9 mmol, 2.44 eq.), ^{n}butyl lithium 2.6 M solution (26.2 mL, 68.7 mmol, 2.22 eq.) and 2,6-bis(chloromethyl)pyridine 4.95 g, 28.1 mmol, 1.00 eq.) was used to afford a white solid (10.47 g, 99 %). ^{1}H NMR (400 MHz, $CDCl_3$) δ 0.01-0.68 (br, m, 6H, P-B$\underline{\boldsymbol{H_3}}$), 1.13-1.19 (m, 12 H, PCH-C$\underline{\boldsymbol{H_3}}$), 2.03-2.16 (m, 4H, P-C$\underline{\boldsymbol{H}}CH_3$), 3.18 (d, J_{HH} = 11.24 Hz, 4H, P-C$\underline{\boldsymbol{H_2}}C_{py}$), 7.20 (d, J_{HH} = 7.7 Hz, 2H, C$_{py}$-$\underline{\boldsymbol{H}_{meta}}$), 7.56 (t, J_{HH} = 7.7 Hz, 1H, C$_{py}$-$\underline{\boldsymbol{H}_{para}}$). ^{13}C{^{1}H} NMR (101 MHz, $CDCl_3$) δ 17.13 (d, J_{PC}= 36.9 Hz, PCH-$\underline{\boldsymbol{C}}H_3$), 21.87 (d, J_{PC} = 31.4 Hz, P-$\underline{\boldsymbol{C}}HCH_3$), 30.54 (d, J_{PC} = 26.5 Hz, P-$\underline{\boldsymbol{C}}H_2C_{py}$), 123.12 ($\underline{\boldsymbol{C}_{py,meta}}$), 136.79 ($\underline{\boldsymbol{C}_{py,para}}$), 154.43 (d, J_{PC}= 5.7 Hz, $\underline{\boldsymbol{C}_{py,ortho}}$). ^{31}P{^{1}H} NMR (162 MHz, $CDCl_3$) δ 35.90, 36.38.

2,6-bis(2-(di-*tert*-butylphosphino-2-propyl)pyridine, Me$_4$PNP^{tBu}. Me$_4$PNP^{tBu}BH$_3$ (500 mg, 1.04 mmol, 1.00 eq.) was put into a dry 100 mL Schlenk flask under Ar, to which 20 mL of pyrrolidine was then added in an N_2 glovebox. The solution was stirred at 90 °C for 18h followed by a thorough evaporation under reduced pressure (0.3Torr) for at least 6 hours to remove all traces of the pyrrolidine-BH$_3$ adduct and unreacted pyrrolidine (use of a second trap is recommended as pyrrolidine is corrosive), giving an off-white solid as the product (450mg, 96%). Colorless crystals suitable for X-ray diffraction study were grown by slow evaporation of a concentrated solution of the ligand in C_6D_6. ^{1}H NMR (400 MHz, C_6D_6): δ 1.19 (d, J_{HP}= 10.0 Hz, 36 H, Me of ^{t}Bu), 1.83 (d, J_{HP} = 6.9 Hz, 12 H, PC-(C$\underline{\boldsymbol{H_3}}$)$_2C_{py}$), 7.17 (t, J_{HH}= 7.9 Hz, 1 H (overlaps with C_6D_6), C$_{py}$-$\underline{\boldsymbol{H}_{para}}$), 7.59 (d, J_{HH}= 7.9 Hz, 2H, C$_{py}$-$\underline{\boldsymbol{H}_{meta}}$). ^{13}C{^{1}H} NMR (101 MHz, C_6D_6): δ 29.35 (br, PC-($\underline{\boldsymbol{C}}H_3$)$_2C_{py}$), 32.46 (d, J_{PC}= 13.8 Hz, Me of ^{t}Bu), 35.10 (d, J_{PC}= 34.7 Hz, C$_{quat}$ of ^{t}Bu), 45.31 (P-$\underline{\boldsymbol{C}}$(CH$_3$)$_2C_{py}$), 121.24 (d, J_{PC}= 16.2 Hz, $\underline{\boldsymbol{C}_{py,meta}}$), 135.03 ($\underline{\boldsymbol{C}_{py,para}}$), 167.30 (d, J_{PC}= 14.6 Hz, $\underline{\boldsymbol{C}_{py,ortho}}$). ^{31}P{^{1}H} NMR (162 MHz, C_6D_6): δ 69.55.

2,6-bis(2-(di-isopropylphosphino-2-propyl)pyridine, boron trihydride adduct, Me$_4$PNP^{iPr}BH$_3$. This ligand was prepared following the same procedure as for the **Me$_4$PNP^{tBu}BH$_3$**. **PNP^{iPr}BH$_3$** (1.00 g, 2.74 mmol, 1.00 eq.), a 2.6 M solution of ^{n}butyl lithium (1.05 mL, 2.74 mmol, 1.00 eq.) and iodomethane (171 µL, 2.74 mmol, 1.00 eq.) were used to prepare the ligand, affording a white crystalline solid (0.96 g, 83%). ^{1}H NMR (400 MHz, $CDCl_3$) δ 0.11-0.59 (br m, 6H, P-B$\underline{\boldsymbol{H_3}}$),0.87 (dd, J_{HP} = 13.0 Hz, J_{HH} = 7.1 Hz, 12H, PCH-C$\underline{\boldsymbol{H_3}}$), 1.17 (dd, J_{HP} = 13.9 Hz, J_{HH} = 7.2 Hz, 12H, PCH-C$\underline{\boldsymbol{H_3}}$), 1.73 (d, J_{HP} = 12.6 Hz, 12H, P-(C$\underline{\boldsymbol{H_3}}$)$_2C_{py}$), 2.13-2.27 (m, 4H, P-C$\underline{\boldsymbol{H}}CH_3$), 7.46 (d, J_{HH} = 8Hz, 2H, C$_{py}$-$\underline{\boldsymbol{H}_{meta}}$), 7.65 (t, J_{HH} = 8 Hz, 1H, C$_{py}$-$\underline{\boldsymbol{H}_{para}}$). ^{13}C{^{1}H} NMR (101 MHz, $CDCl_3$) δ 18.34 (PCH-$\underline{\boldsymbol{C}}H_3$), 19.23 (PCH-$\underline{\boldsymbol{C}}H_3$), 22.14 (d, J_{PC}= 28 Hz, P-$\underline{\boldsymbol{C}}HCH_3$), 26.66 (PC-($\underline{\boldsymbol{C}}H_3$)$_2C_{py}$), 41.35 (d, J_{PC}=21.7 Hz, P-$\underline{\boldsymbol{C}}$(CH$_3$)$_2C_{py}$), 121.28 ($\underline{\boldsymbol{C}_{py,meta}}$), 136.89 ($\underline{\boldsymbol{C}_{py,para}}$), 167.77 ($\underline{\boldsymbol{C}_{py,ortho}}$). ^{31}P{^{1}H} NMR (162 MHz, $CDCl_3$) δ 50.78, 50.29. ESI-HRMS (m/z) calculated for [$C_{23}H_{49}NB_2P_2$ + H$^+$] = 424.3599. Found for [$C_{23}H_{50}NB_2P_2$ + H$^+$] = 424.3603. UV-vis (CH_2Cl_2, [1·10^{-4} M]), λ_{max}, nm (ε, L·mol^{-1}·cm^{-1}): 269 (7670). Anal. Calcd. For $C_{23}H_{49}B_2NP_2$: C, 65.27; H, 11.66; N, 3.31. Found: C, 65.22; H, 11.79; N, 3.84.

2,6-bis(2-(di-isopropylphosphino-2-propyl)pyridine, Me_4PNP^{iPr}. **$Me_4PNP^{iPr}BH_3$** (40 mg, 0.095 mmol, 1.0 eq.) was put into a dry 50 mL Schlenk flask under Ar and 10 mL of pyrrolidine (under N_2) was added. The solution was stirred at 90 °C for 18h followed by a thorough evaporation under reduced pressure for at least 6 hours to remove all traces of the pyrrolidine-BH_3 adduct (use of a second trap is recommended as pyrrolidine is corrosive), giving a viscous colorless oil as the product (38 mg, 100%). ^{1}H NMR (400 MHz, C_6D_6) δ 0.90 (dd, J_{HP} = 10.1 Hz, J_{HH} = 7.1 Hz, 12H, PCH-C***H*****$_3$**), 1.15 (dd, J_{HP}= 14.2 Hz, J_{HH}= 7.3 Hz, 12H, PCH-C***H*****$_3$**), 1.65 (d, J_{HH} = 10.1 Hz, 12H, PC-(C***H*****$_3$)$_2$C$_{py}$), 1.75-1.87 (m, 4H, P-C***H***CH$_3$), 7.13 (s, 3H, C$_{py}$-***H*****$_{meta}$** + C$_{py}$-***H*****$_{para}$**). ^{13}C{^{1}H} NMR (101 MHz, C_6D_6) δ 20.36 (d, J_{PC}= 9.9 Hz, PCH-(***C***H$_3$)$_2$), 22.68 (d, J_{PC} = 23.3 Hz, P-***C***H(CH$_3$)$_2$), 23.48 (d, J_{PC}= 22.1 Hz, PCH-(***C***H$_3$)$_2$), 27.53 (d, J_{PC}= 13.7 Hz, PC-(***C***H$_3$)$_2$C$_{py}$), 41.49 (d, J_{PC}=24.3 Hz, P-***C***(CH$_3$)$_2$C$_{py}$), 118.58 (d, J_{PC}= 8.1 Hz, ***C*****$_{py,meta}$**), 135.67 (***C*****$_{py,para}$**), 165.71 (d, J_{PC} =5.0 Hz, ***C*****$_{py,ortho}$**). ^{31}P{^{1}H} NMR (162 MHz, C_6D_6) δ 43.46.

[(Me_4PNP^{iPr})Ni^{II}Br][Br], [1]Br. **$Me_4PNP^{iPr}BH_3$** (400 mg, 1.01 mmol, 1.00 eq.) was added to a pre-dried Schlenk flask under Ar and approximately 15 mL of pyrrolidine was added to this flask inside a glovebox after which time it was sealed and taken outside. The reaction is stirred for 24 hours at 100 °C and then the pyrrolidine is evaporated under reduced pressure for at least 6 hours (use of a second trap is recommended as pyrrolidine is corrosive). The resulting deprotected ligand was a viscous oil that was taken back inside the glovebox and used directly without isolation for the metalation reaction, assuming a 100% conversion to deprotected form. 20 mL of dry THF was added to the oil, followed by anhydrous nickel(II) bromide (232 mg, 1.06 mmol, 1.05 eq.). The mixture was stirred and heated at 60 °C overnight. After cooling, a cannula was used to remove the dark liquid residue to give a solid that was washed two times with hexanes and evaporated under reduced pressure to give a brown-orange powder (388 mg, 62%). Orange crystals suitable for X-ray diffraction were obtained by slow evaporation from an acetone solution of **[1]Br** at-30 °C. ^{1}H NMR (400 MHz, $CDCl_3$) δ 1.23-1.29 (m, 12H, PCH-C***H*****$_3$**), 1.55-1.60 (m, 12H, PCH-C***H*****$_3$**), 1.83-1.86 (m, 12 H, PC-C***H*****$_3$**C$_{py}$), 2.52–2.65 (m, 4H, P-C***H***CH$_3$), 7.74 (d, J_{HH} = 7.8 Hz, 2H, C$_{py}$-***H*****$_{meta}$**), 8.54 (t, J_{HH}= 8.1 Hz, 1H, C$_{py}$-***H*****$_{para}$**). ^{13}C{^{1}H} NMR (101 MHz, $CDCl_3$) δ 19.26, (PCH-***C***H$_3$), 19.79 (PCH-***C***H$_3$), 23.45 (vt, J_{PC} = 10.8 Hz, P-***C***HCH$_3$), 28.35 (PC-(***C***H$_3$)$_2$C$_{py}$), 50.44 (vt, J_{PC} = 8.1 Hz, P-***C***(CH$_3$)$_2$C$_{py}$), 121.76 (vt, J_{PC} = 4.4 Hz, ***C*****$_{py,meta}$**), 145.20 (***C*****$_{py,para}$**), 172.74 (vt, J_{PC} = 7.2 Hz, ***C*****$_{py,ortho}$**). ^{31}P{^{1}H} NMR (162 MHz, $CDCl_3$) δ 73.82. UV-vis (CH_2Cl_2, [1·10^{-4} M]), λ_{max}, nm (ε, L·mol^{-1}·cm^{-1}): 261 (10100), 303 (3400), 347 (8240), 468 (1130). ATR-IR (cm^{-1}): 3039 (w), 2965 (m), 2896 (w), 2872 (w), 1589 (m), 1559 (w), 1455 (s), 1389 (s), 1367 (s), 1292 (s), 1241 (s), 1164 (w), 1133 (w), 1096 (w), 1034 (m), 1012 (w), 928 (m), 888 (m), 831 (s), 752 (w), 715 (w), 664 (s). ESI-HRMS (m/z) calculated for $[C_{23}H_{43}NNiP_2Br]^+$ = 534.15. Found for $[C_{23}H_{43}NNiP_2Br]^+$ = 534.1367. Anal. Calcd. For $C_{23}H_4Br_2NP_2Ni$: C, 44.99; H, 7.06; N, 2.28. Found: C, 44.98; H, 7.04; N, 2.33.

[(Me_4PNP^{iPr})Ni^{II}Cl][Cl], [2]Cl. The procedure to prepare **[1]Br** was also used to prepare **[2]Cl**. **$Me_4PNP^{iPr}BH_3$** ligand (500 mg, 1.18 mmol, 1.00 eq.), and anhydrous nickel(II) chloride (153 mg, 1.18 mmol, 1.00 eq.) were used to afford a light yellow powder (427 mg, 69 % yield). Crystals suitable for X-ray diffraction studies were obtained by vapor diffusion of hexanes into a concentrated solution of **[2]Cl** in benzene at rt. Although stable under air, the product complex is highly hygroscopic, and as it was taken out of, and used outside the glovebox, water molecules were present in the elemental analysis and NMR, as well as in the X-ray structure.^{1}H NMR. (400 MHz, acetone-d_6) δ 1.34 (d, J_{HH} = 7.0 Hz, 12H, PCH-C***H*****$_3$**), 1.60 (d, J_{HH} = 7.0 Hz, 12H, PCH-C***H*****$_3$**), 1.92 (br s, 12H, P-C(C***H*****$_3$)$_2$C$_{py}$), 2.61–2.72 (hept, $^3J_{HH}$ = 7 Hz, 4H, P-C***H***CH$_3$), 7.78 (d, J_{HH} = 7.7 Hz, 2H, C$_{py}$-***H*****$_{meta}$**), 8.35 (t, J_{HH} = 7.7 Hz, 1H, C$_{py}$-***H*****$_{para}$**). ^{13}C{^{1}H} NMR (101 MHz, acetone-d_6) δ 19.26 (PCH-(***C***H$_3$)$_2$), 19.63 (PCH-(***C***H$_3$)$_2$), 23.67 (P-***C***H(CH$_3$)$_2$), 28.17 (PC-(***C***H$_3$)$_2$C$_{py}$), 50.52 (P-***C***(CH$_3$)$_2$C$_{py}$), 122.20 (***C*****$_{py,meta}$**), 144.76 (***C*****$_{py,para}$**), 174.23 (***C*****$_{py,ortho}$**). Water present in hygroscopic sample of **[2]Cl** was detected by NMR and X-ray. ^{31}P{^{1}H} NMR (162 MHz, $CDCl_3$) δ 71.38. UV-vis (CH_2Cl_2, 1·10^{-4} M]), λ_{max}, nm (ε, L mol^{-1} cm^{-1}): 259 (5430), 305 (3520), 338 (6970), 452 (903). ATR-IR (cm^{-1}): 2963 (m), 2871 (m), 1592 (w), 1563 (w), 1454 (s), 1387 (m), 1638 (m), 1268 (w), 1167 (w), 1126 (w), 1099 (w), 1072 (w), 1032 (m), 931 (m), 884 (m), 828 (m), 759 (m), 696 (w), 665 (s). ESI-HRMS (m/z) calculated for $[C_{23}H_{43}NNiP_2Cl]^+$= 488.1904. Found for $[C_{23}H_{43}NNiP_2Cl]^+$ = 488.1895. Anal. Calcd. For $C_{23}H_{43}Cl_2NP_2Ni\cdot H_2O$: C, 50.86; H, 8.35; N, 2.58 (according to X-ray, one water molecule per complex present in the crystalline sample of **[2Cl]**). Found: C, 49.74; H, 8.13; N, 2.69. Deviation of %C could be due to hygroscopic nature of complex.

[(Me_4PNP^{tBu})Pyridine)Ni^{II}Br][Br], [3]Br. The analogous procedure to prepare **[1]Br** was used to prepare **[3]Br**. **$Me_4PNP^{tBu}BH_3$** (359 mg, 0.749 mmol, 1.00 eq.) and anhydrous nickel(II) bromide (164 mg, 0.749 mmol, 1.00 eq.) are reacted to afford a dark red powder (288 mg, 57%). Red crystals suitable for X-ray diffraction were obtained by slow evaporation of an acetone solution of **[3]Br** at rt. ^{1}H NMR (400 MHz, acetone-d_6) δ 1.51-1.54 (br m, 18H, Me of ^{t}Bu), 1.65-1.92 (br m, 18H, Me of ^{t}Bu), 2.08-2.12 (br m, 6H, PC-(C***H*****$_3$)$_2$C$_{py}$), 2.18-2.21 (br m, 6H, P-C(C***H*****$_3$)$_2$C$_{py}$), 7.73 (d, J_{HH} = 8 Hz, 2H, C$_{py}$-***H*****$_{meta}$**), 8.34 (tt, J_{HH} = 8.0 Hz, J_{HP} = 1.6 Hz, 1H, C$_{py}$-***H*****$_{para}$**). ^{13}C{^{1}H} NMR (101 MHz, acetone-d_6) δ 24.98 (P-C(***C***H$_3$)$_2$C$_{py}$), 32.20 (Me of ^{t}Bu), 32.89 (br, Me of ^{t}Bu), 36.00 (P-C(***C***H$_3$)$_2$C$_{py}$), 40.11 (C$_{quat}$ of ^{t}Bu), 41.52 (C$_{quat}$ of ^{t}Bu), 53.32 (P-***C***(CH$_3$)$_2$C$_{py}$), 121.93 (***C*****$_{py,meta}$**), 145.04 (***C*****$_{py,para}$**), 173.87 (***C*****$_{py,ortho}$**). ^{31}P{^{1}H} (162 MHz, acetone-d_6) δ 87.00. ATR-IR (cm^{-1}): 3425 (w), 3377 (w), 2959 (m), 2903 (m), 2114 (w), 2080 (w), 1593 (m), 1457 (m), 1395 (s), 1365 (m), 1168 (s), 1019 (m), 935 (m), 919 (m), 829 (m), 806 (m), 767 (m), 745 (m). UV-vis (CH_2Cl_2, [1·10^{-4} M]), λ_{max}, nm (ε, L mol^{-1} cm^{-1}): 263 (15600), 363 (8820). 505 (1740). Anal. Calcd. For $C_{27}H_{51}NP_2NiBr_2$: C, 48.39; H, 7.67; N, 2.09. Found: C, 47.95; H, 7.29; N, 2.19.

[(Me_4PNP^{tBu})Pyridine)Ni^{II}Cl][Cl], [4]Cl. The same procedure to prepare **[3]Br** was used to prepare **[4]Cl**. **$Me_4PNP^{tBu}BH_3$** ligand (500 mg, 1.04 mmol, 1.00 eq.), and anhydrous nickel(II) chloride (135 mg, 1.04 mmol, 1.00 eq.) was used to afford a bright orange powder (516 mg, 85.0% yield). Crystals suitable for X-ray diffraction studies were obtained by vapor diffusion of hexanes into a concentrated THF solution of **[4]Cl** at rt. ^{1}H NMR (600 MHz, acetone-d_6) δ 1.43-1.61 (br m, 18H, Me of ^{t}Bu), 1.65-1.91 (br m, Me of ^{t}Bu), 2.06-2.13 (br m, 6H, P-C(C***H*****$_3$)$_2$C$_{py}$), 2.14-2.24 (br m, 6H, P-C(C***H*****$_3$)$_2$C$_{py}$), 7.77 (d, J_{HH} = 8.0 Hz, 2H, C$_{py}$-***H*****$_{meta}$**), 8.35 (t, J_{HH} = 8.0 Hz, C$_{py}$-***H*****$_{para}$**). Water present in hygroscopic sample of **[2]Cl** is confirmed by X-ray diffraction as one molecule of water. ^{13}C{^{1}H} NMR (151 MHz, acetone-d_6) δ 24.61 (PC-(***C***H$_3$)$_2$C$_{py}$), 31.89 (br, Me of ^{t}Bu), 35.93 (br, PC-(***C***H$_3$)$_2$C$_{py}$), 39.95 (br, C$_{quat}$ of ^{t}Bu), 40.64 (br, C$_{quat}$ of ^{t}Bu), 52.82 (vt, J_{PC} =

5.4 Hz, P-**C**$(CH_3)_2C_{py}$), 121.86 (**C**$_{py,meta}$), 145.10 (**C**$_{py,para}$), 174.17 (**C**$_{py,ortho}$). $^{31}P\{^1H\}$ (262 MHz, acetone-d_6) = 83.63. ATR-IR (cm^{-1}): 2977 (m), 2962 (m), 2906 (m), 2872 (m), 1596 (w), 1565 (w), 1459 (s), 1395 (m), 1363 (s), 1276 (m), 1172 (s), 1136 (w), 1106 (w), 1067 (s), 1020 (m), 923 (m), 831 (w), 810 (m), 761 (m), 710 (w), 662 (w). UV-vis (CH_2Cl_2, [$1\cdot10^{-4}$ M]), λ_{max}, nm (ε, L mol^{-1} cm^{-1}): 256 (7620), 308 (sh, 2980), 351 (9580), 481 (1360). ESI-HRMS (m/z) calculated for $[C_{27}H_{51}NNiP_2Cl]^+$= 544.2533. Found for $[C_{27}H_{51}NNiP_2Cl]^+$ = 544.2520. Anal. Calcd. For $C_{27}H_{51}NP_2NiCl_2$+ 1 H_2O: C, 54.12; H, 8.91; N, 2.34. Found: C, 54.08; H, 8.90; N, 2.44. According to X-ray analysis, one water molecule per complex was present in crystalline sample of **[4]Cl**.

[(Me$_4$PNP^{iPr})Ni^{II}Br][B(3,5-$CF_3C_6H_3)_4$], [1]B(Ar^F)$_4$. To a solution of **[1]Br** (10.0 mg, 0.0163 mmol, 1.00 eq.) in 10 mL of dry THF in an N_2 glovebox at room temperature, sodium tetrakis[3,5-bis(trifluoromethyl)phenyl]borate (14.7 mg, 0.0163 mmol, 1.00 eq.) was added and the solution was agitated by hand for 5 minutes. Then, the solution was filtered through a small celite plug and concentrated under reduced pressure to afford a light orange solid (24 mg, 100%). Crystals suitable for X-ray diffraction analysis were obtained by vapor diffusion of hexanes into a concentrated THF solution of **[1]B(Ar^F)$_4$** at RT. ^1H NMR (400 MHz, acetone-d_6) δ 1.31-1.36 (m, 12H, PCH-C**H$_3$**), 1.58-1.64 (m, 6H, PCH-C**H$_3$**), 1.89-1.91 (m, 12H, PC-C**H$_3$**C_{py}), 2.68-2.78 (m, 4H, P-C**H**CH_3), 7.66 (br m, 6H total, BC_{Ar}-**H$_{para}$** (4H) + C_{py}-**H$_{meta}$** (2H)), 7.78 (br m, 8H, BC_{Ar}-**H$_{ortho}$**), 8.31 (tt, J_{HH} = 8.0 Hz, J_{PH} = 1.3 Hz, 1H, C_{py}-**H$_{para}$**). $^{13}C\{^1H\}$ NMR (101 MHz, acetone-d_6) δ 19.31 (PCH-**C**H_3), 19.91 (PCH-**C**H_3), 24.08 (vt, J_{PC} = 11.2 Hz,P-**C**HCH_3), 28.29 (PC-(**C**$H_3)_2C_{py}$), 51.08 (vt, J_{PC} = 8.4, Hz, P-**C**$(CH_3)_2C_{py}$), 118.46 (m, B-**C$_{Ar,para}$**), 121.85 (vt, J_{PC} = 4.4 Hz, **C$_{py,meta}$**), 125.37 (q, J_{CF} = 273.1 Hz, $BC_{Ar,meta}$-**C**F_3), 130.02 (m, B-**C$_{Ar,meta}$**CF_3), 135.53 (B-**C$_{Ar,ortho}$**), 144.45 (**C$_{py,para}$**), 162.59 (dd, J_{BC} = 50.0 Hz, B-**C$_{Ar,ipso}$**), 174.36 (vt, J_{PC} = 7.1 Hz, **C$_{py,ortho}$**). $^{31}P\{^1H\}$ NMR (162 MHz, acetone-d_6) δ 74.73. ^{19}F NMR (376.2 MHz, acetone-d_6) δ -63.13. ATR-IR (cm^{-1}): 2972 (w), 1610 (w), 1459 (w), 1353 (m), 1272 (s), 1115 (s), 885 (m), 839 (m), 715 (m), 682 (m), 668 (m). UV-vis (CH_2Cl_2, [$1\cdot10^{-4}$ M]), λ_{max}, nm (ε, L mol^{-1} cm^{-1}): 262 (13100), 279 (sh, 7120), 307 (3030), 348 (7300), 469 (1040). Anal. Calcd. For $C_{55}H_{55}NP_2NiBrBF_{24}$: C, 47.27; H, 3.97; N, 1.00. Found: C, 45.38; H, 3.45; N, 1.38. Despite multiple attempts, we were unable to obtain satisfactory elemental analysis for this compound.

[(Me$_4$PNP^{iPr})Ni^{II}Cl][B(3,5-$CF_3C_6H_3)_4$], [2]B(Ar^F)$_4$. To a solution of **[2]Cl** (100 mg, 0.190 mmol, 1.00 eq.) in 10 mL of dry THF in an N_2 glovebox at room temperature, sodium tetrakis[3,5-bis(trifluoromethyl)phenyl]borate (169 mg, 0.190 mmol, 1.00 eq.) was added and the solution was stirred for an hour. The reaction mixture was filtered through a small celite plug and concentrated under reduced pressure. The solid was then washed with approximately 3 mL of diethyl ether to afford an orange solid (226 mg, 88 %). Crystals suitable for X-ray diffraction were obtained by vapor diffusion of hexanes into a concentrated THF solution of **[2]B(Ar^F)$_4$** at RT. ^1H NMR (400 MHz, acetone-d_6) δ 1.30-1.35 (m, 12H, PCH-C**H$_3$**), 1.56-1.62 (m, 12H, PCH-C**H$_3$**), 1.88-1.90 (m, 12 H, PC-C**H$_3$**C_{py}), 2.57-2.70 (m, 4H, P-C**H**CH_3), 2.77 (br s, 1H, **H**DO), 2.81 (br s, 1.5H, **H$_2$**O) 7.62 (d, J_{HH} = 8.1 Hz, C_{py}-**H$_{meta}$**), 7.64 (br s, 4H, BC_{Ar}-**H$_{para}$**), 7.75-7.76 (m, 8H, BC_{Ar}-**H$_{ortho}$**), 8.26 (tt, J_{HH} = 7.9 Hz, J_{HP} = 1.3 Hz, 1H, C_{py}-**H$_{para}$**). $^{13}C\{^1H\}$ NMR (101 MHz, acetone-d_6) δ 19.20 (PCH-(**C**$H_3)_2$), 19.59 (PCH-(**C**$H_3)_2$), 23.66 (vt, J_{PC} = 10.6 Hz, P-**C**$H(CH_3)_2$), 28.12 (PC-(**C**$H_3)_2C_{py}$), 50.52 (vt, J_{PC} = 8.30 Hz, P-**C**$(CH_3)_2C_{py}$), 118.46 (m, B-**C$_{Ar,para}$**), 121.85 (vt, J_{PC} = 3.03 Hz, **C$_{py,meta}$**), 125.37 (q, J_{CF} = 273.2 Hz, $BC_{Ar,meta}$-**C**F_3), 130.01 (qdd, J_{CF} = 31.0 Hz; J_{CB} = 5.3 Hz; J_{CF}= 2.8 Hz, B-**C$_{Ar,meta}$**CF_3), 135.53 (B-**C$_{Ar,ortho}$**), 144.40 (**C$_{py,para}$**), 162.59 (dd, J_{BC} = 50.0 Hz, B-**C$_{Ar,ipso}$**), 174.45 (vt, J_{PC} = 7.47 Hz, **C$_{py,ortho}$**). $^{31}P\{^1H\}$ NMR (162 MHz, acetone-d_6) δ 72.23. ^{19}F NMR (376.2 MHz, acetone-d_6) δ -63.14. ATR-IR (cm^{-1}): 2974 (w), 1606 (w), 1465 (w), 1394 (w), 1354 (m), 1273 (s), 1160 (m), 1119 (s), 1035 (w), 931 (w), 885 (m), 838 (w), 813 (w), 752 (w), 713 (m), 670 (m). UV-vis (CH_2Cl_2, [$1\cdot10^{-4}$ M]), λ_{max}, nm (ε, L mol^{-1} cm^{-1}): 260 (12500), 279 (sh, 6100), 307 (sh, 5650), 339 (11000), 454 (1410). ESI-HRMS (m/z) calculated for $[C_{23}H_{43}NNiP_2Cl]^+$= 488.1904 and for $[C_{32}H_{12}BF_{24}]^-$ = 863.0643. Found for $[C_{23}H_{43}NNiP_2Cl]^+$ = 488.1900 and for $[C_{32}H_{12}BF_{24}]^-$ = 863.0643. Anal. Calcd. For $C_{55}H_{55}BClF_{24}NNiP_2$: C, 48.83; H, 4.10; N, 1.04. Found: C, 48.5; H, 4.07; N, 1.15.

[(Me$_4$PNP^{tBu})Ni^{II}Br][B(3,5-$CF_3C_6H_3)_4$], [3]B(Ar^F)$_4$. [3]Br (20.0 mg, 0.0298 mmol, 1.00 eq) was dissolved in dry toluene in a 20 mL vial in the Ar glovebox. A few drops of anhydrous CH_2Cl_2 were added to facilitate dissolution. Sodium tetrakis[3,5-bis(trifluoromethyl)phenyl]borate (26.4 mg, 0.298 mmol, 1.00 eq) was added and the mixture agitated for 5 minutes. The solution was filtered through a short celite plug, then concentrated to give the pure product as a light pink solid (35 mg, 80 %). Red crystals of diffraction quality were obtained by liquid diffusion of pentane into a concentrated THF solution of **[3]B(Ar^F)$_4$** at -30 °C. ^1H NMR (600 MHz, acetone-d_6) δ 1.48-1.56 (br m, 18H, Me of ^{t}Bu), 1.70-1.87 (br m, 18H, Me of ^{t}Bu), 2.07-2.11 (br m, 6H, PC-(C**H$_3$**)C_{py}), 2.17-2.22 (br m, 6H, PC-(C**H$_3$**)$_2C_{py}$), 7.64 (d, J_{HH} = 7.9 Hz, 2H, C_{py}-**H$_{meta}$**), 7.66 (br s, 4 H, BC_{Ar}-**H$_{para}$**), 7.77-7.78 (br m, 8H, BC_{Ar}-**H$_{ortho}$**), 8.28 (t, J_{HH} = 7.9 Hz, 1H, C_{py}-**H$_{para}$**). $^{13}C\{^1H\}$ NMR (151 MHz, acetone-d_6) δ 24.87 (PC-(**C**$H_3)_2C_{py}$), 32.20 (Me of ^{t}Bu), 33.04 (br, Me of ^{t}Bu), 36.07 (PC-(**C**$H_3)_2C_{py}$), 40.15 (C_{quat} of ^{t}Bu), 41.62 (C_{quat} of ^{t}Bu), 53.28 (vt, J_{PC} = 4.4 Hz, P-**C**$(CH_3)_2C_{py}$), 118.46 (m, B-**C$_{Ar,para}$**), 121.60 (br, **C$_{py,meta}$**), 125.38 (q, J_{CF} = 272.0 Hz, $BC_{Ar,meta}$-**C**F_3), 130.01 (qdd, J_{CF} = 31.7 Hz; J_{CB} = 5.2 Hz; J_{CF}= 2.6 Hz, B-**C$_{Ar,meta}$**CF_3), 135.54 (B-**C$_{Ar,ortho}$**), 144.64 (**C$_{py,para}$**), 162.61 (q, J_{BC} = Hz, 50.0 Hz, B-**C$_{Ar,ipso}$**), 174.14 (**C$_{py,ortho}$**). $^{31}P\{^1H\}$ NMR (242.95 MHz, acetone-d_6) δ 87.28. $^{19}F\{^1H\}$ NMR (564.73 MHz, acetone-d_6) δ -63.15. ATR-IR (cm^{-1}): 3005 (w), 2976 (w), 2914 (w), 1605 (w), 1482 (w), 1397 (w), 1353 (m), 1273 (s), 1121 (s), 1017 (w), 928 (w), 888 (m), 838 (w), 806 (w), 746 (w), 714 (m), 871 (m). UV-vis (CH_2Cl_2, [$1\cdot10^{-4}$ M]), λ_{max}, nm (ε, L mol^{-1} cm^{-1}) : 263 (9860), 363 (4370), 505 (811). ESI-HRMS (m/z) calculated for $[C_{27}H_{51}NNiP_2Br]^+$= 588.2028 and for $[C_{32}H_{12}BF_{24}]^-$ = 863.0643 Found for $[C_{27}H_{51}NNiP_2Br]^+$ = 588.2014 and for $[C_{32}H_{12}BF_{24}]^-$ = 863.0569. Anal. Calcd. For $C_{59}H_{63}B_1Br_1F_{24}N_1P_2Ni_1$: C, 48.76; H, 4.37; N, 0.96. Found: C, 48.66; H, 4.34; N, 1.12.

[(Me$_4$PNP^{tBu})Ni^{II}Cl][B(3,5-$CF_3C_6H_3)_4$], [4]B(Ar^F)$_4$. To a solution of **[4]**Cl (100 mg, 0.172 mmol, 1.00 eq.) in 10 mL of anhydrous THF in an N_2 glovebox at room temperature, sodium tetrakis[3,5-bis(trifluoromethyl)phenyl]borate (152 mg, 0.172 mmol, 1.00 eq.) was added and the solution was stirred for an hour. The reaction mixture was filtered through a small celite plug and concentrated under reduced pressure. The solid was subsequently washed with approximately 3 mL of diethyl ether to afford an orange solid (163 mg, 67 %). ^1H NMR (600 MHz, acetone-d_6) δ 1.44-1.61 (br m, 18H, Me of ^{t}Bu), 1.64-1.91 (br m, 18H, Me of ^{t}Bu), 2.05-2.11 (br m, 6H, PC-(C**H$_3$**)$_2C_{py}$), 2.15-2.23 (br m, 6H, PC-(C**H$_3$**)$_2C_{py}$), 7.60 (d, J_{HH}

= 8.1 Hz, 2H, C_{py}-***H*****$_{meta}$**), 7.66 (br s, 4 H, BC_{Ar}-***H*****$_{para}$**), 7.77-7.79 (m, 8H, BC_{Ar}-***H*****$_{ortho}$**), 8.25 (tt, J_{HH} = 8.1 Hz, J_{HP} = 1.1 Hz, 1H, C_{py}-***H*****$_{para}$**). $^{13}C\{^1H\}$ NMR (151 MHz, acetone-d_6) δ 24.53 (br, PC-(***C***H_3)$_2C_{py}$), 31.89 (br, Me of ^{t}Bu), 36.04 (br, PC-(***C***H_3)$_2C_{py}$), 40.03 (br, C_{quat} of ^{t}Bu), 40.79 (br, C_{quat} of ^{t}Bu), 52.77 (vt, J_{PC} = 4.8 Hz, P-***C***$(CH_3)_2C_{py}$), 118.43-118.49 (m, B-***C*****$_{Ar,para}$**), 121.39 (br, ***C*****$_{py,meta}$**), 125.40 (q, J_{CF} = 272.0 Hz, BC_{Ar}-***C***F_3), 130.04 (qdd, J_{CF} = 31.7 Hz; J_{CB} = 5.2 Hz; J_{CF}= 2.7 Hz, B-***C*****$_{Ar,meta}$**CF_3), 135.56 (B-***C*****$_{Ar,ortho}$**), 144.59 (***C*****$_{py,para}$**), 162.62 (dd, J_{BC} = 49.83 Hz, B-***C*****$_{Ar,ipso}$**), 174.46 (***C*****$_{py,ortho}$**). $^{31}P\{^1H\}$ NMR (242.95 MHz, acetone-d_6) δ 83.92. $^{19}F\{^1H\}$ NMR (564.73 MHz, acetone-d_6) δ -63.14. ATR-IR (cm^{-1}): 2975 (w), 2912 (w), 1743 (w), 1606 (w), 1569 (w), 1486 (w), 1396 (w), 1353 (m), 1273 (s), 1119 (s), 1018 (w), 929 (w), 887 (m), 837 (w), 806 (w), 745 (w), 713 (m), 672 (m). UV-vis (CH_2Cl_2, [1·10^{-4} M]), λ_{max}, nm (ε, L mol^{-1} cm^{-1}): 261 (15700), 278 (sh, 7590), 309 (sh, 4260), 351 (14000), 481 (1910). ESI-HRMS (m/z) calculated for $[C_{27}H_{51}NNiP_2Cl]^+$= 544.2533 and for $[C_{32}H_{12}BF_{24}]^-$ = 863.0643 Found for $[C_{23}H_{43}NNiP_2Cl]^+$ = 544.2525 and for $[C_{32}H_{12}BF_{24}]^-$ = 863.0638. Anal. Calcd. For $C_{59}H_{63}BClF_{24}NNiP_2$: C, 50.29; H, 4.51; N, 0.99. Found: C, 48.93; H, 4.15; N, 1.10.

(Me$_4$PNP^{iPr})Ni^{I}Br, 5. Method 1: Chemical reduction using $CoCp_2$. To a solution of **[1]Br** (50.0 mg, 0.081 mmol, 1.00 eq.) in dry acetone, cobaltocene (15.4 mg, 0.081 mmol, 1.00 eq.) was added at room temperature. The solution turns dark red immediately and after 5 minutes of stirring, the mixture was filtered through a short celite plug. The acetone was evaporated to afford a red solid (34.5 mg, 79% yield). Red crystals suitable for X-ray diffraction were obtained by cooling down a solution of **5** acetone-d_6 at -30 °C under nitrogen atmosphere. Crystals of the complex in in acetone or MeTHF mixture was characterized by EPR spectroscopy (see main text). ^{1}H NMR (400 MHz, C_6D_6): δ 44.01 (br), 34.38 (br s), 5.02 (br s), 4.02 (br s), 1.56 (s), -0.20 (br s), -51.45 (br s). ATR-IR (cm^{-1}): 3055 (w), 2954 (s), 2923 (m), 2866 (s), 2717 (w), 2110 (w), 2073 (w), 1888 (w), 1809 (w), 1709 (w), 1581 (w), 1559 (w), 1452 (s), 1382 (m), 1296 (w), 1231 (m), 1183 (w), 1156 (w), 1084 (w), 1035 (m), 1003 (m), 954 (w), 928 (w), 867 (m), 808(s), 746 (s), 663 (s). UV-vis (THF, [1·10^{-4} M]), λ_{max}, nm (ε, L mol^{-1} cm^{-1}): 237 (9630), 263 (10700), 298 (sh, 6650), 464 (1430), 529 (941).

Method 2: Generation of Ni^1 complex by electrochemical reduction and coulometric analysis. Ni^I complex **5** was prepared via bulk electrolysis at the same time as a coulometric analysis was performed. A voltage of -1500 mV was applied (using an $Ag/AgNO_3$ reference electrode, a platinum gauze working electrode and a platinum gauze counter-electrode) to a yellow solution of **[1]B(Ar^F)$_4$** (1·10^{-3}M using 0.1M ^{n}Bu$_4$NPF$_6$ in dry CH_3CN as the electrolyte). The voltage was applied for 1830 s, until the current measured was less than 1% of the starting current (charge measured = 0.800 C, theoretical charge for 1 electron reduction = 0.771 C). At that point the solution had become brown. The nature of the product formed was confirmed by comparing its low temperature EPR spectra and g tensor values with those from the chemically reduced **5** (see main text).

(Me$_4$PNP^{iPr})Ni^{I}Cl, 6. The complex was prepared via method 1 described for the preparation of complex **5** above, using the following quantities: **[2]Cl** (70.0 mg, 0.133 mmol, 1.00 eq.) and cobaltocene (25.2 mg, 0.133 mmol, 1.00 eq.) gave a dark red powder (55.4 mg, 85%). Red crystals of **6** were obtained in the same way as described in method 1 for the preparation of **5**. The complex solution in 20% acetone/MeTHF was analyzed by EPR spectroscopy (See main text). ^{1}H NMR (400 MHz, C_6D_6): δ 44.07 (br), 36.64 (br s), 4.77 (br s), 3.92 (br s), 3.11 (s), 0.30 (br s), -51.52 (br s). ATR-IR (cm^{-1}): 3069 (w), 2983 (m), 2960 (m), 2943 (m), 2922(m), 2893 (m), 1712 (w), 1584 (w), 1539 (w), 1464 (m), 1451 (m), 1413 (m), 1388 (m), 1380 (m), 1364 (w), 1234 (w), 1220 (w), 1188 (w), 1156 (w), 1109 (w), 1087 (w), 1040 (m), 1016 (w), 996 (m), 958 (w), 950 (w), 925 (w), 895 (w), 879 (m), 810 (m), 779 (s), 753 (s), 732 (w), 668 (s). UV-vis (THF, [1·10^{-4} M]), λ_{max}, nm (ε, L mol^{-1} cm^{-1}): 233 (19200), 260 (16200), 294 (sh, 9680), 338 (9440), 480 (1070). Anal. Calcd. For $C_{23}H_{43}ClNNiP_2$: C, 56.41; H, 8.85; N, 2.86. Found: C, 55.81 H, 7.75; N, 2.27

(Me$_4$PNP^{tBu})Pyridine)Ni^{I}Br, 7. The complex was prepared following method 1 used to prepare complex **5** using the following quantities: **[3]Br** (40.0 mg, 0.060 mmol, 1.00 eq.) and cobaltocene (11.3 mg, 0.060 mmol, 1.00 eq.) and gave a red powder (26.1 mg, 65% yield). Dark orange crystals of complex **7** were obtained by crystallization of a concentrated solution in acetone-d_6 at -30 °C under a nitrogen atmosphere. The complex solution in 35% acetone/MeTHF was analyzed by EPR spectroscopy (See main text). ^{1}H NMR (400 MHz, C_6D_6): δ 11.12 (br s), 5.24 (br s), 1.97 (br s), -51.50 (br s). ATR-IR (cm^{-1}): 3329 (w), 3057 (w), 2991 (m), 2955 (m), 2891 (m), 2864 (m), 2708 (w), 2656 (w), 2111 (w), 1701 (w), 1558 (w), 1486 (m), 1443 (m), 1388 (s), 1359 (m), 1251 (w), 1217 (w), 1172 (m), 1106 (m), 995 (m), 947 (w), 931 (w), 891 (w), 858 (w), 808 (m), 776 (s), 757 (s), 726 (w), 680 (w). UV-vis (THF, [1·10^{-4} M]), λ_{max}, nm (ε, L mol^{-1} cm^{-1}): 261 (12000), 328 (8840), 499 (1100).

(Me$_4$PNP^{tBu})Ni^{I}Cl, 8. The complex was prepared via method 1 described for the preparation of complex **5** above, except that a 2 hour mixing time was needed, using the following quantities: **[4]Cl** (25.0 mg, 0.043 mmol, 1.00 eq.) and cobaltocene (8.1 mg, 0.043 mmol, 1.00 eq.). A dark red powder (20.7 mg, 88 % yield) was obtained. Dark red crystals of **8** were obtained in the same way as described in method 1 for the preparation of **5**. The complex solution in MeTHF was analyzed by EPR spectroscopy (See main text). ^{1}H NMR (400 MHz, C_6D_6): δ 12.09 (br s), 6.23 (br s), -51.52 (br s). ATR-IR (Solid state, cm^{-1}): 3057 (w), 2979 (m), 2960 (m), 2894 (m), 2872 (m), 1702 (m), 1595 (m), 1579 (w), 1563 (w), 1470 (m), 1461 (m), 1450 (m), 1409 (w), 1395 (m), 1364 (m), 1253 (m), 1212 (w), 1196 (w), 1171 (m), 1137 (m), 1107 (m), 1018 (m), 987 (w), 978 (m), 932 (w), 903 (w), 891 (w), 831 (m), 806 (s), 763 (m), 758 (m), 746 (m), 724 (w), 661 (m), 654 (m). UV-vis (THF, [1·10^{-4} M]), λ_{max}, nm (ε, L mol^{-1} cm^{-1}): 267 (12800), 334 (3220), 462 (508)

ASSOCIATED CONTENT

Supporting Information

The Supporting Information is available free of charge on the ACS Publications website: experimental details, characterization data, computational details and xyz coordinates. Complete details or the X-ray analysis reported herein have been deposited at the Cambridge Crystallographic Data Center (CCDC 1885748 (**Me$_4$PNP^{iPr}BH$_3$**), 1885747 (**Me$_4$PNP^{tBu}BH$_3$**), 1885755 (**Me$_4$PNP^{tBu}**), 1885758 (**[1]Br**), 1885751 (**[2]Cl**), 1885754 (**[3]Br**), 1885752 (**[4]Cl**), 1885750 (**[1]B(Ar^F)$_4$**), 1885757 (**[2]B(Ar^F)$_4$**), 1885759 (**[3]B(Ar^F)$_4$**), 1885756 (**[4]B(Ar^F)$_4$**), 1885745 (**5**), 1885749 (**6**), 1885746 (**7**), 1885753 (**8**)). These data can be obtained free of charge via www.ccdc.cam.ac.uk/data_request/cif, by e-mailing da-

ta_request@ccdc.cam.ac.uk, or by contacting the Cambridge Crystallographic Data Centre, 12 Union Road, Cambridge, CD2 1EZ, UK; fax: +44 1223 336033.

Corresponding Author

* E-mail: juliak@oist.jp (J.R.K.)

ORCID

Sébastien Lapointe: 0000-0003-3190-3803

Eugene Khaskin: 0000-0003-1790-704X

Robert R. Fayzullin: 0000-0002-3740-9833

Julia R. Khusnutdinova: 0000-0002-5911-4382

Notes

The authors declare no competing financial interests.

ACKNOWLEDGMENT

We thank Dr. Michael Roy for technical support for NMR, mass spectrometry, and elemental analysis (OIST). We also thank Dr. Yukio Mizuta (JEOL RESONANCE Inc.) for helpful discussions regarding EPR measurements and simulation, Dr. Shrinwantu Pal (University of British Columbia) and Prof Ilya Gridnev (Tohoku University) for suggestions regarding DFT calculations. We also thank Dr. Orestes Rivada-Wheelagan and Dr Abhishek Dubey for helpful discussions. The authors acknowledge the Okinawa Institute of Science and Technology Graduate University for start-up funding and for access to its high performance cluster facility.

REFERENCES

1. Moulton, C. J.; Shaw, B. L., Transition metal–carbon bonds. Part XLII. Complexes of nickel, palladium, platinum, rhodium and iridium with the tridentate ligand 2,6-bis[(di-t-butylphosphino)methyl]phenyl. *J. Chem. Soc., Dalton Trans.* **1976**, 1020-1024.

2. van Koten, G.; Timmer, K.; Noltes, J. G.; Spek, A. L., A novel type of Pt-C interaction and a model for the final stage in reductive elimination processes involving C-C coupling at Pt; synthesis and molecular geometry of [1,N,N'-ε-2,6-bis{(dimethylamino)methyl}-toluene]iodoplatinum(II) tetrafluoroborate. *J. Chem. Soc., Chem. Commun.* **1978**, 250-252.

3. van Koten, G.; Jastrzebski, J. T. B. H.; Noltes, J. G.; Spek, A. L.; Schoone, J. C., Triorganotin cations stabilized by intramolecular Sn-N coordination; synthesis and characterization of {C,N,N′ -2,6-bis[(dimethylamino)methyl]phenyl}diorganotin bromides. *J. Organomet. Chem.* **1978,** *148*, 233-245.

4. Castonguay, A.; Sui-Seng, C.; Zargarian, D.; Beauchamp, A. L., Syntheses and Reactivities of New $PC_{sp3}P$ Pincer Complexes of Nickel. *Organometallics* **2006,** *25*, 602-608.

5. Kennedy, A. R.; Cross, R. J.; Muir, K. W., Preparation and crystal structure of trans-[$NiBr\{C_6H_3$-2,6-$(CH_2PCy_2)_2\}$]. *Inorg. Chim. Acta* **1995,** *231*, 195-200.

6. Huck, W. T. S.; Snellink-Rueel, B.; van Veggel, F. C. J. M.; Reinhoudt, D. N., New Building Blocks for the Noncovalent Assembly of homo- and hetero-Multinuclear Metallodendrimers. *Organometallics* **1997,** *16*, 4287-4291.

7. Kozhanov, K. A.; Bubnov, M. P.; Cherkasov, V. K.; Vavilina, N. N.; Efremova, L. Y.; Artyushin, O. I.; Odinets, I. L.; Abakumov, G. A., o-Semiquinonic PCP-pincer nickel complexes with alkyl substituents: versatile coordination sphere dynamics. *Dalton Trans.* **2008**, 2849-2853.

8. Kozhanov, K. A.; Bubnov, M. P.; Cherkasov, V. K.; Fukin, G. K.; Abakumov, G. A., An EPR study of the intramolecular dynamics in o-semiquinonic nickel complexes with a diphosphorous pincer ligand. *Chem. Commun.* **2003**, 2610-2611.

9. Campora, J.; Palma, P.; Del Rio, D.; Alvarez, E., CO Insertion Reactions into the M-OH Bonds of Monomeric Nickel and Palladium Hydroxides. Reversible Decarbonylation of a Hydroxycarbonyl Palladium Complex. *Organometallics* **2004,** *23*, 1652-1655.

10. Campora, J.; Palma, P.; del Rio, D.; Mar Conejo, M.; Alvarez, E., Synthesis and Reactivity of a Mononuclear Parent Amido Nickel Complex. Structures of $Ni[C_6H_3$-2,6-$(CH_2PiPr_2)_2](NH_2)$ and $Ni[C_6H_3$-2,6-$(CH_2PiPr_2)_2](OMe)$. *Organometallics* **2004,** *23*, 5653-5655.

11. Boro, B. J.; Duesler, E. N.; Goldberg, K. I.; Kemp, R. A., Synthesis, Characterization, and Reactivity of Nickel Hydride Complexes Containing 2,6-$C_6H_3(CH_2PR_2)_2$ (R = ^{t}Bu, ^{c}Hex, and ^{i}Pr) Pincer Ligands. *Inorg. Chem.* **2009,** *48*, 5081-5087.

12. Groux, L. F.; Belanger-Gariepy, F.; Zargarian, D., Phosphino-indenyl complexes of nickel(II). *Can. J. Chem.* **2005,** *83*, 634-639.

13. Schmeier, T. J.; Hazari, N.; Incarvito, C. D.; Raskatov, J. A., Exploring the reactions of CO_2 with PCP supported nickel complexes. *Chem. Commun.* **2011,** *47*, 1824-1826.

14. Levina, V. A.; Rossin, A.; Belkova, N. V.; Chierotti, M. R.; Epstein, L. M.; Filippov, O. A.; Gobetto, R.; Gonsalvi, L.; Lledos, A.; Shubina, E. S.; Zanobini, F.; Peruzzini, M., Acid-Base Interaction between Transition-Metal Hydrides: Dihydrogen Bonding and Dihydrogen Evolution. *Angew. Chem., Int. Ed.* **2011,** *50*, 1367-1370.

15. van der Boom, M. E.; Liou, S.-Y.; Shimon, L. J. W.; Ben-David, Y.; Milstein, D., Nickel promoted C-H, C-C and C-O bond activation in solution. *Inorg. Chim. Acta* **2004,** *357*, 4015-4023.

16. Gomez-Benitez, V.; Baldovino-Pantaleon, O.; Herrera-Alvarez, C.; Toscano, R. A.; Morales-Morales, D., High yield thiolation of iodobenzene catalyzed by the phosphinite nickel PCP pincer complex: $[NiCl\{C_6H_3$-2,6-$(OPPh_2)_2\}]$. *Tetrahedron Lett.* **2006,** *47*, 5059-5062.

17. Vabre, B.; Lindeperg, F.; Zargarian, D., Direct, one-pot synthesis of POCOP-type pincer complexes from metallic nickel. *Green Chem.* **2013,** *15*, 3188-3194.

18. Lapointe, S.; Vabre, B.; Zargarian, D., POCOP-Type Pincer Complexes of Nickel: Synthesis, Characterization, and Ligand Exchange Reactivities of New Cationic Acetonitrile Adducts. *Organometallics* **2015,** *34*, 3520-3531.

19. Estudiante-Negrete, F.; Hernandez-Ortega, S.; Morales-Morales, D., Ni(II)-POCOP pincer compound $[NiCl\{C_{10}H_5$-2,10-$(OPPh_2)_2\}]$ an efficient and robust nickel catalyst for the Suzuki-Miyaura coupling reactions. *Inorg. Chim. Acta* **2012,** *387*, 58-63.

20. Chakraborty, S.; Krause, J. A.; Guan, H., Hydrosilylation of Aldehydes and Ketones Catalyzed by Nickel PCP-Pincer Hydride Complexes. *Organometallics* **2009,** *28*, 582-586.

21. Zhang, J.; Medley, C. M.; Krause, J. A.; Guan, H., Mechanistic Insights into C-S Cross-Coupling Reactions Catalyzed by Nickel Bis(phosphinite) Pincer Complexes. *Organometallics* **2010,** *29*, 6393-6401.

22. Chakraborty, S.; Patel, Y. J.; Krause, J. A.; Guan, H., Catalytic properties of nickel bis(phosphinite) pincer complexes in the reduction of CO_2 to methanol derivatives. *Polyhedron* **2012,** *32*, 30-34.

23. Pandarus, V.; Zargarian, D., New Pincer-Type Diphosphinito (POCOP) Complexes of Nickel. *Organometallics* **2007,** *26*, 4321-4334.

24. Spasyuk, D. M.; Zargarian, D.; van der Est, A., New POCN-Type Pincer Complexes of Nickel(II) and Nickel(III). *Organometallics* **2009,** *28*, 6531-6540.

25. Zhang, B.-S.; Wang, W.; Shao, D.-D.; Hao, X.-Q.; Gong, J.-F.; Song, M.-P., Unsymmetrical Chiral PCN Pincer Palladium(II) and Nickel(II) Complexes of (Imidazolinyl)aryl Phosphinite Ligands: Synthesis via Ligand C-H Activation, Crystal Structures, and Catalytic Studies. *Organometallics* **2010,** *29*, 2579-2587.

26. Spasyuk, D. M.; Gorelsky, S. I.; van der Est, A.; Zargarian, D., Characterization of Divalent and Trivalent Species Generated in the Chemical and Electrochemical Oxidation of a Dimeric Pincer Complex of Nickel. *Inorg. Chem.* **2011,** *50*, 2661-2674.
27. Yang, M.-J.; Liu, Y.-J.; Gong, J.-F.; Song, M.-P., Unsymmetrical Chiral PCN Pincer Palladium(II) and Nickel(II) Complexes with Aryl-Based Aminophosphine-Imidazoline Ligands: Synthesis via Aryl C-H Activation and Asymmetric Addition of Diarylphosphines to Enones. *Organometallics* **2011,** *30*, 3793-3803.
28. Sanford, J.; Dent, C.; Masuda, J. D.; Xia, A., Synthesis, characterization and application of pincer-type nickel iminophosphinite complexes. *Polyhedron* **2011,** *30*, 1091-1094.
29. Fan, L.; Foxman, B. M.; Ozerov, O. V., N-H Cleavage as a Route to Palladium Complexes of a New PNP Pincer Ligand. *Organometallics* **2004,** *23*, 326-328.
30. Ozerov, O. V.; Guo, C.; Fan, L.; Foxman, B. M., Oxidative Addition of N-C and N-H Bonds to Zerovalent Nickel, Palladium, and Platinum. *Organometallics* **2004,** *23*, 5573-5580.
31. Liang, L.-C.; Chien, P.-S.; Huang, Y.-L., Intermolecular Arene C-H Activation by Nickel(II). *J. Am. Chem. Soc.* **2006,** *128*, 15562-15563.
32. Liang, L.-C.; Chien, P.-S.; Lin, J.-M.; Huang, M.-H.; Huang, Y.-L.; Liao, J.-H., Amido Pincer Complexes of Nickel(II): Synthesis, Structure, and Reactivity. *Organometallics* **2006,** *25*, 1399-1411.
33. Adhikari, D.; Huffman, J. C.; Mindiola, D. J., Structural elucidation of a nickel boryl complex. A recyclable borylation Ni(II) reagent of bromobenzene. *Chem. Commun.* **2007**, 4489-4491.
34. Adhikari, D.; Pink, M.; Mindiola, D. J., Mild protocol for the synthesis of stable nickel complexes having primary and secondary silyl ligands. *Organometallics* **2009,** *28*, 2072-2077.
35. Fryzuk, M. D.; Montgomery, C. D., Amides of the platinum group metals. *Coord. Chem. Rev.* **1989,** *95*, 1-40.
36. Ingleson, M. J.; Fullmer, B. C.; Buschhorn, D. T.; Fan, H.; Pink, M.; Huffman, J. C.; Caulton, K. G., Influence of the d-Electron Count on CO Binding by Three-Coordinate $[(^tBu_2PCH_2SiMe_2)_2N]Fe$, -Co, and -Ni. *Inorg. Chem.* **2008,** *47*, 407-409.
37. Fryzuk, M. D.; MacNeil, P. A., Hybrid multidentate ligands. Tridentate amidophosphine complexes of nickel(II) and palladium(II). *J. Am. Chem. Soc.* **1981,** *103*, 3592-3.
38. Tondreau, A. M.; Boncella, J. M., The synthesis of PNP-supported low-spin nitro manganese(I) carbonyl complexes. *Polyhedron* **2016,** *116*, 96-104.
39. Abdul Goni, M.; Rosenberg, E.; Meregude, S.; Abbott, G., A methods study of immobilization of PONOP pincer transition metal complexes on silica polyamine composites (SPC). *J. Organomet. Chem.* **2016,** *807*, 1-10.
40. Castro-Rodrigo, R.; Chakraborty, S.; Munjanja, L.; Brennessel, W. W.; Jones, W. D., Synthesis, Characterization, and Reactivities of Molybdenum and Tungsten PONOP Pincer Complexes. *Organometallics* **2016,** *35*, 3124-3131.
41. DeRieux, W.-S. W.; Wong, A.; Schrodi, Y., Synthesis and characterization of iron complexes based on bis-phosphinite PONOP and bis-phosphite PONOP pincer ligands. *J. Organomet. Chem.* **2014,** *772-773*, 60-67.
42. Kundu, S.; Brennessel, W. W.; Jones, W. D., Synthesis and Reactivity of New Ni, Pd, and Pt 2,6-Bis(di-tert-butylphosphinito)pyridine Pincer Complexes. *Inorg. Chem.* **2011,** *50*, 9443-9453.
43. Kundu, S.; Brennessel, W. W.; Jones, W. D., Making M-CN bonds from M-Cl in (PONOP)M and (dippe)Ni systems (M = Ni, Pd, and Pt) using t-BuNC. *Inorg. Chim. Acta* **2011,** *379*, 109-114.
44. Salem, H.; Shimon, L. J. W.; Diskin-Posner, Y.; Leitus, G.; Ben-David, Y.; Milstein, D., Formation of Stable trans-Dihydride Ruthenium(II) and 16-Electron Ruthenium(0) Complexes Based on Phosphinite PONOP Pincer Ligands. Reactivity toward Water and Electrophiles. *Organometallics* **2009,** *28*, 4791-4806.
45. Barloy, L.; Malaise, G.; Ramdeehul, S.; Newton, C.; Osborn, J. A.; Kyritsakas, N., Synthesis and Structural Studies of Binuclear Platinum(II) Complexes with a Novel Phosphorus-Nitrogen-Phosphorus Ligand. *Inorg. Chem.* **2003,** *42*, 2902-2907.
46. Vabre, B.; Canac, Y.; Duhayon, C.; Chauvin, R.; Zargarian, D., Nickel(II) complexes of the new pincer-type unsymmetrical ligands PIMCOP, PIMIOCOP, and NHCCOP: versatile binding motifs. *Chem. Commun.* **2012,** *48*, 10446-10448.
47. Vechorkin, O.; Proust, V.; Hu, X., Functional Group Tolerant Kumada-Corriu-Tamao Coupling of Nonactivated Alkyl Halides with Aryl and Heteroaryl Nucleophiles: Catalysis by a Nickel Pincer Complex Permits the Coupling of Functionalized Grignard Reagents. *J. Am. Chem. Soc.* **2009,** *131*, 9756-9766.
48. Madhira, V. N.; Ren, P.; Vechorkin, O.; Hu, X.; Vicic, D. A., Synthesis and electronic properties of a pentafluoroethyl-derivatized nickel pincer complex. *Dalton Trans.* **2012,** *41*, 7915-7919.
49. Breitenfeld, J.; Scopelliti, R.; Hu, X., Synthesis, Reactivity, and Catalytic Application of a Nickel Pincer Hydride Complex. *Organometallics* **2012,** *31*, 2128-2136.
50. Martinez, G. E.; Ocampo, C.; Park, Y. J.; Fout, A. R., Accessing Pincer Bis(carbene) Ni(IV) Complexes from Ni(II) via Halogen and Halogen Surrogates. *J. Am. Chem. Soc.* **2016,** *138*, 4290-4293.
51. Kozhanov, K. A.; Bubnov, M. P.; Cherkasov, V. K.; Fukin, G. K.; Vavilina, N. N.; Efremova, L. Y.; Abakumov, G. A., First structurally characterized mixed-halogen nickel(III) NCN-pincer complex. *J. Magn. Res.* **2009,** *197*, 36-39.
52. Himmelbauer, D.; Mastalir, M.; Stöger, B.; Veiros, L. F.; Pignitter, M.; Somoza, V.; Kirchner, K., Iron PCP Pincer Complexes in Three Oxidation States: Reversible Ligand Protonation To Afford an Fe(0) Complex with an Agostic C–H Arene Bond. *Inorg. Chem.* **2018,** *57*, 7925-7931.
53. Danopoulos, A. A.; Wright, J. A.; Motherwell, W. B.; Ellwood, S., N-Heterocyclic "Pincer" Dicarbene Complexes of Cobalt(I), Cobalt(II), and Cobalt(III). *Organometallics* **2004,** *23*, 4807-4810.
54. Monfette, S.; Turner, Z. R.; Semproni, S. P.; Chirik, P. J., Enantiopure C1-Symmetric Bis(imino)pyridine Cobalt Complexes for Asymmetric Alkene Hydrogenation. *J. Am. Chem. Soc.* **2012,** *134*, 4561-4564.
55. Ito, M.; Matsumoto, T.; Tatsumi, K., Synthesis and reactions of mono- and dinuclear Ni(I) thiolate complexes. *Inorg. Chem.* **2009,** *48*, 2215-2223.
56. Yoo, C.; Oh, S.; Kim, J.; Lee, Y., Transmethylation of a four-coordinate nickel(I) monocarbonyl species with methyl iodide. *Chem. Sci.* **2014,** *5*, 3853-3858.
57. Blackaby, W. J. M.; Sabater, S.; Poulten, R. C.; Page, M. J.; Folli, A.; Krewald, V.; Mahon, M. F.; Murphy, D. M.; Richards, E.; Whittlesey, M. K., Mono- and dinuclear Ni(I) products formed upon bromide abstraction from the Ni(I) ring-expanded NHC complex $[Ni(6\text{-}Mes)(PPh_3)Br]$. *Dalton Trans.* **2018,** *47*, 769-782.
58. Chakraborty, U.; Urban, F.; Mühldorf, B.; Rebreyend, C.; de Bruin, B.; van Velzen, N.; Harder, S.; Wolf, R., Accessing the CpArNi(I) Synthon: Reactions with N-Heterocyclic Carbenes, TEMPO, Sulfur, and Selenium. *Organometallics* **2016,** *35*, 1624-1631.
59. Chakraborty, U.; Mühldorf, B.; van Velzen, N. J. C.; de Bruin, B.; Harder, S.; Wolf, R., [CpArNi{Ga(nacnac)}]: An Open-Shell Nickel(I) Complex Supported by a Gallium(I)

Carbenoid (CpAr = $C_5(C_6H_4$-4-Et$)_5$, nacnac = HC[C(Me)N-(C_6H_3)-2,6-i$Pr_2]_2$). *Inorg. Chem.* **2016,** *55*, 3075-3078.
60. Grueger, N.; Wadepohl, H.; Gade, L. H., A readily accessible PNP pincer ligand with a pyrrole backbone and its NiI/II chemistry. *Dalton Trans.* **2012,** *41*, 14028-14030.
61. Zimmermann, P.; Limberg, C., Activation of Small Molecules at Nickel(I) Moieties. *J. Am. Chem. Soc.* **2017,** *139*, 4233-4242.
62. Yao, S.; Driess, M., Lessons from isolable nickel(I) precursor complexes for small molecule activation. *Acc Chem Res* **2012,** *45*, 276-87.
63. Kieber-Emmons, M. T.; Riordan, C. G., Dioxygen Activation at Monovalent Nickel. *Acc. Chem. Res.* **2007,** *40*, 618-625.
64. Pelties, S.; Herrmann, D.; de Bruin, B.; Hartl, F. e.; Wolf, R., Selective P_4 activation by an organometallic nickel(I) radical: formation of a dinuclear nickel(II) tetraphosphide and related di- and trichalcogenides. *Chem. Commun.* **2014,** *50*, 7014-7016.
65. Rettenmeier, C. A.; Wadepohl, H.; Gade, L. H., Electronic structure and reactivity of nickel(I) pincer complexes: their aerobic transformation to peroxo species and site selective C-H oxygenation. *Chem. Sci.* **2016,** *7*, 3533-3542.
66. Tondreau, A. M.; Atienza, C. C. H.; Weller, K. J.; Nye, S. A.; Lewis, K. M.; Delis, J. G. P.; Chirik, P. J., Iron Catalysts for Selective Anti-Markovnikov Alkene Hydrosilylation Using Tertiary Silanes. *Science* **2012,** *335*, 567-570.
67. Ruddy, A. J.; Kelly, C. M.; Crawford, S. M.; Wheaton, C. A.; Sydora, O. L.; Small, B. L.; Stradiotto, M.; Turculet, L., (N-Phosphinoamidinate)Iron Pre-Catalysts for the Room Temperature Hydrosilylation of Carbonyl Compounds with Broad Substrate Scope at Low Loadings. *Organometallics* **2013,** *32*, 5581-5588.
68. Langlotz, B. K.; Wadepohl, H.; Gade, L. H., Chiral Bis(pyridylimino)isoindoles: A Highly Modular Class of Pincer Ligands for Enantioselective Catalysis. *Angew. Chem. Int. Ed.* **2008,** *47*, 4670-4674.
69. Rettenmeier, C.; Wadepohl, H.; Gade, L. H., Stereoselective Hydrodehalogenation via a Radical-Based Mechanism Involving T-Shaped Chiral Nickel(I) Pincer Complexes. *Chem. - Eur. J.* **2014,** *20*, 9657-9665.
70. Matsubara, K.; Fukahori, Y.; Inatomi, T.; Tazaki, S.; Yamada, Y.; Koga, Y.; Kanegawa, S.; Nakamura, T., Monomeric Three-Coordinate N-Heterocyclic Carbene Nickel(I) Complexes: Synthesis, Structures, and Catalytic Applications in Cross-Coupling Reactions. *Organometallics* **2016,** *35*, 3281-3287.
71. Matsubara, K.; Yamamoto, H.; Miyazaki, S.; Inatomi, T.; Nonaka, K.; Koga, Y.; Yamada, Y.; Veiros, L. F.; Kirchner, K., Dinuclear Systems in the Efficient Nickel-Catalyzed Kumada-Tamao-Corriu Cross-Coupling of Aryl Halides. *Organometallics* **2017,** *36*, 255-265.
72. Miyazaki, S.; Koga, Y.; Matsumoto, T.; Matsubara, K., A new aspect of nickel-catalyzed Grignard cross-coupling reactions: selective synthesis, structure, and catalytic behavior of a T-shape three-coordinate nickel(I) chloride bearing a bulky NHC ligand. *Chem. Commun.* **2010,** *46*, 1932-1934.
73. Duñach, E.; Medeiros, M. J.; Olivero, S., Electrochemical cyclizations of organic halides catalyzed by electrogenerated nickel(I) complexes: towards environmentally friendly methodologies. *Electrochim. Acta* **2017,** *242*, 373-381.
74. Zuo, Z.; Ahneman, D. T.; Chu, L.; Terrett, J. A.; Doyle, A. G.; MacMillan, D. W. C., Merging photoredox with nickel catalysis: Coupling of α-carboxyl sp_3-carbons with aryl halides. *Science* **2014,** *345*, 437-440.
75. Rettenmeier, C. A.; Wenz, J.; Wadepohl, H.; Gade, L. H., Activation of Aryl Halides by Nickel(I) Pincer Complexes: Reaction Pathways of Stoichiometric and Catalytic Dehalogenations. *Inorg. Chem.* **2016,** *55*, 8214-8224.
76. Lin, C.-Y.; Power, P. P., Complexes of Ni(I): a "rare" oxidation state of growing importance. *Chemical Society Reviews* **2017,** *46*, 5347-5399.
77. Niklas, J.; Westwood, M.; Mardis, K. L.; Brown, T. L.; Pitts-McCoy, A. M.; Hopkins, M. D.; Poluektov, O. G., X-ray Crystallographic, Multifrequency Electron Paramagnetic Resonance, and Density Functional Theory Characterization of the Ni($PCy_2NtBu_2)_2^{n+}$ Hydrogen Oxidation Catalyst in the Ni(I) Oxidation State. *Inorg. Chem.* **2015,** *54*, 6226-6234.
78. Vogt, M.; de Bruin, B.; Berke, H.; Trincado, M.; Grützmacher, H., Amino olefin nickel(I) and nickel(0) complexes as dehydrogenation catalysts for amine boranes. *Chem. Sci.* **2011,** *2*, 723-727.
79. Iffland, L.; Petuker, A.; van Gastel, M.; Apfel, U.-P., Mechanistic Implications for the Ni(I)-Catalyzed Kumada Cross-Coupling Reaction. *Inorganics* **2017,** *5*.
80. Dürr, A. B.; Fisher, H. C.; Kalvet, I.; Truong, K.-N.; Schoenebeck, F., Divergent Reactivity of a Dinuclear (NHC)Nickel(I) Catalyst versus Nickel(0) Enables Chemoselective Trifluoromethylselenolation. *Angew. Chem. Int. Ed.* **2017,** *56*, 13431-13435.
81. Anderson, T. J.; Jones, G. D.; Vicic, D. A., Evidence for a Ni(I) Active Species in the Catalytic Cross-Coupling of Alkyl Electrophiles. *J. Am. Chem. Soc.* **2004,** *126*, 8100-8101.
82. Breitenfeld, J.; Ruiz, J.; Wodrich, M. D.; Hu, X., Bimetallic Oxidative Addition Involving Radical Intermediates in Nickel-Catalyzed Alkyl–Alkyl Kumada Coupling Reactions. *J. Am. Chem. Soc.* **2013,** *135*, 12004-12012.
83. Brazzolotto, D.; Gennari, M.; Queyriaux, N.; Simmons, T. R.; Pécaut, J.; Demeshko, S.; Meyer, F.; Orio, M.; Artero, V.; Duboc, C., Nickel-centred proton reduction catalysis in a model of [NiFe] hydrogenase. *Nat Chem* **2016,** *8*, 1054-1060.
84. Sarangi, R.; Dey, M.; Ragsdale, S. W., Geometric and Electronic Structures of the Ni(I) and Methyl−Ni(III) Intermediates of Methyl-Coenzyme M Reductase. *Biochemistry* **2009,** *48*, 3146-3156.
85. Bender, G.; Pierce, E.; Hill, J. A.; Darty, J. E.; Ragsdale, S. W., Metal centers in the anaerobic microbial metabolism of CO and CO_2. *Metallomics* **2011,** *3*, 797-815.
86. Seravalli, J.; Ragsdale, S. W., Pulse-Chase Studies of the Synthesis of Acetyl-CoA by Carbon Monoxide Dehydrogenase/Acetyl-CoA Synthase: Evidence for a random mechanism of methyl and carbonyl addition. *J. Biol. Chem.* **2008,** *283*, 8384-8394.
87. George, S. J.; Seravalli, J.; Ragsdale, S. W., EPR and Infrared Spectroscopic Evidence That a Kinetically Competent Paramagnetic Intermediate is Formed When Acetyl-Coenzyme A Synthase Reacts with CO. *J. Am. Chem. Soc.* **2005,** *127*, 13500-13501.
88. Ragsdale, S. W., Life with Carbon Monoxide. *Crit. Rev. Biochem. Mol. Biol.* **2004,** *39*, 165-195.
89. Jiang, Y.; Gendy, C.; Roesler, R., Nickel, Ruthenium, and Rhodium NCN-Pincer Complexes Featuring a Six-Membered N-Heterocyclic Carbene Central Moiety and Pyridyl Pendant Arms. *Organometallics* **2018,** *37*, 1123-1132.
90. Kozhanov, K. A.; Bubnov, M. P.; Cherkasov, V. K.; Abakumov, G. A., EPR study of spin-labeled nickel NCN-pincer complexes. *Dokl. Chem.* **2006,** *407*, 35-38.
91. Lescot, C.; Savourey, S.; Thuery, P.; Lefevre, G.; Berthet, J.-C.; Cantat, T., Synthesis, structure and electrochemical behavior of new RPONOP (R = tBu, iPr) pincer complexes of Fe^{2+}, Co^{2+}, Ni^{2+}, and Zn^{2+} ions. *C. R. Chim.* **2016,** *19*, 57-70.
92. Yoo, C.; Lee, Y., A T-Shaped Nickel(I) Metalloradical Species. *Angew Chem Int Ed Engl* **2017,** *56*, 9502-9506.
93. Mastalir, M.; Kirchner, K., A triazine-based Ni(II) PNP pincer complex as catalyst for Kumada-Corriu and Negishi cross-coupling reactions. *Monatsh. Chem.* **2017,** *148*, 105-109.

94. Mastalir, M.; Stoeger, B.; Pittenauer, E.; Allmaier, G.; Kirchner, K., Air-Stable Triazine-Based Ni(II) PNP Pincer Complexes As Catalysts for the Suzuki-Miyaura Cross-Coupling. *Org. Lett.* **2016,** *18*, 3186-3189.
95. Shih, W.-C.; Ozerov, O. In *One pot synthesis of arene-based PCP/PNP ligands and corresponding nickel complexes*2015 American Chemical Society; pp INOR-767.
96. Oren, D.; Diskin-Posner, Y.; Avram, L.; Feller, M.; Milstein, D., Metal–Ligand Cooperation as Key in Formation of Dearomatized Ni(II)–H Pincer Complexes and in Their Reactivity toward CO and CO_2. *Organometallics* **2018,** *37*, 2217-2221.
97. Holmes, A. J.; Rayner, P. J.; Cowley, M. J.; Green, G. G. R.; Whitwood, A. C.; Duckett, S. B., The reaction of an iridium PNP complex with parahydrogen facilitates polarisation transfer without chemical change. *Dalton Trans.* **2015,** *44*, 1077-1083.
98. Miyake, Y.; Nakajima, K.; Higuchi, Y.; Nishibayashi, Y., Synthesis and Redox Properties of PNP Pincer Complexes Based on N-Methyl-4,4'-bipyridinium. *Eur. J. Inorg. Chem.* **2014,** *2014*, 4273-4280.
99. Rosiak, D.; Okuniewski, A.; Chojnacki, J., Novel complexes possessing Hg–(Cl, Br, I)···OC halogen bonding and unusual $Hg_2S_2(Br/I)_4$ kernel. The usefulness of τ_4' structural parameter. *Polyhedron* **2018,** *146*, 35-41.
100. Yang, L.; Powell, D. R.; Houser, R. P., Structural variation in copper(i) complexes with pyridylmethylamide ligands: structural analysis with a new four-coordinate geometry index, τ4. *Dalton Trans.* **2007**, 955-964.
101. Okuniewski, A.; Rosiak, D.; Chojnacki, J.; Becker, B., Coordination polymers and molecular structures among complexes of mercury(II) halides with selected 1-benzoylthioureas. *Polyhedron* **2015,** *90*, 47-57.
102. Bondi, A., van der Waals Volumes and Radii. *J. Phys. Chem.* **1964,** *68*, 441-451.
103. Guzei, I. A.; Wendt, M., An improved method for the computation of ligand steric effects based on solid angles. *Dalton Trans.* **2006**, 3991-3999.
104. Bilbrey, J. A.; Kazez, A. H.; Locklin, J.; Allen, W. D., Exact Ligand Solid Angles. *J. Chem. Theory Comput.* **2013,** *9*, 5734-5744.
105. Frew, J. J. R.; Damian, K.; Van Rensburg, H.; Slawin, A. M. Z.; Tooze, R. P.; Clarke, M. L., Palladium(II) Complexes of New Bulky Bidentate Phosphanes: Active and Highly Regioselective Catalysts for the Hydroxycarbonylation of Styrene. *Chem. Eur. J.* **2009,** *15*, 10504-10513.
106. Naghipour, A.; Sabounchei, S. J.; Morales-Morales, D.; Hernández-Ortega, S.; Jensen, C. M., Synthesis of a new class of unsymmetrical PCP′ pincer ligands and their palladium (II) complexes: X-ray structure determination of $PdCl\{C_6H_3\text{-}2\text{-}CH_2PPh_2\text{-}6\text{-}CH_2PtBu_2\}$. *J. Organomet. Chem.* **2004,** *689*, 2494-2502.
107. Sheldrick, G., SHELXT - Integrated space-group and crystal-structure determination. *Acta Crystallogr., Sect. A* **2015,** *71*, 3-8.
108. Sheldrick, G., Crystal structure refinement with SHELXL. *Acta Crystallogr., Sect. C* **2015,** *71*, 3-8.
109. Holmes, A. J.; Rayner, P. J.; Cowley, M. J.; Green, G. G. R.; Whitwood, A. C.; Duckett, S. B., The reaction of an iridium PNP complex with parahydrogen facilitates polarisation transfer without chemical change. *Dalton Trans.* **2015,** *44*, 1077-1083.